

A rational length scale for large-eddy simulation of turbulence on anisotropic grids

F.X.Trias,^{1, a)} J.Ruano,^{1, b)} A.Duben,^{2, c)} and A.Gorobets^{2, d)}

¹⁾*Heat and Mass Transfer Technological Center, Technical University of Catalonia, c/Colom 11, 08222 Terrassa, Spain*

²⁾*Keldysh Institute of Applied Mathematics, 4A, Miusskaya Sq., Moscow 125047, Russia*

(Dated: 30 December 2025)

Due to the prohibitive cost of resolving all relevant scales, direct numerical simulations of turbulence remain unfeasible for most real-world applications. Consequently, dynamically simplified formulations are needed for coarse-grained simulations. In this regard, eddy-viscosity models for Large-Eddy Simulation (LES) are widely used both in academia and industry. These models require a subgrid characteristic length, typically linked to the local grid size. While this length scale corresponds to the mesh step for isotropic grids, its definition for unstructured or anisotropic Cartesian meshes, such as the pancake-like meshes commonly used to capture near-wall turbulence or shear layers, remains an open question. Despite its significant influence on LES model performance, no consensus has been reached on its proper formulation. In this work, we introduce a novel subgrid characteristic length. This length scale is derived from the analysis of the entanglement between the numerical discretization and the filtering in LES. Its mathematical properties and simplicity make it a robust choice for reducing the impact of mesh anisotropies on simulation accuracy. The effectiveness of the proposed subgrid length is demonstrated through simulations of decaying isotropic turbulence and a turbulent channel flow using different codes.

^{a)}francesc.xavier.trias@upc.edu

^{b)}jesus.ruano@upc.edu

^{c)}aduben@keldysh.ru

^{d)}gorobets@keldysh.ru

I. INTRODUCTION

Direct numerical simulations (DNS) of the Navier–Stokes (NS) equations remain impractical for most real-world turbulent flows because not enough resolution is available to resolve all the relevant scales of motion. Therefore, practical numerical simulations have to resort to turbulence modeling. Hence, we may turn to large-eddy simulation (LES) to predict the large-scale behavior of turbulent flows: namely, the large scales are explicitly computed, whereas effects of small scale motions are modeled. Shortly, the LES equations for incompressible flows are obtained by applying a spatial filter to the NS equations

$$\partial_t \bar{\mathbf{u}} + (\bar{\mathbf{u}} \cdot \nabla) \bar{\mathbf{u}} = \nu \nabla^2 \bar{\mathbf{u}} - \nabla \bar{p} - \nabla \cdot \tau; \quad \nabla \cdot \bar{\mathbf{u}} = 0, \quad (1)$$

where $\bar{\mathbf{u}}$ denotes the filtered velocity, and the subgrid-scale (SGS) stress tensor is given by $\tau = \overline{\mathbf{u} \otimes \mathbf{u}} - \bar{\mathbf{u}} \otimes \bar{\mathbf{u}}$, where \otimes denotes the standard tensor product of vectors. The filter $\mathbf{u} \rightarrow \bar{\mathbf{u}}$, with filter length δ , is assumed to be symmetric and to commute with differentiation. Notice that τ depends on both the filtered velocity, $\bar{\mathbf{u}}$, and the full velocity field, \mathbf{u} , leading to a closure problem. Therefore, τ is approximated by a tensor that only depends on the filtered velocity, *i.e.*, $\tau \approx \tau(\bar{\mathbf{u}})$.

The eddy-viscosity assumption continues to be the dominant approach for closure modeling, primarily due to its simplicity and robustness,

$$\tau(\bar{\mathbf{u}}) \approx -2\nu_t \mathbf{S}(\bar{\mathbf{u}}), \quad (2)$$

where ν_t is the eddy viscosity, and $\mathbf{S}(\bar{\mathbf{u}}) = \frac{1}{2}(\nabla \bar{\mathbf{u}} + \nabla \bar{\mathbf{u}}^T)$ is the rate-of-strain tensor. The SGS tensor, $\tau(\bar{\mathbf{u}})$, is considered traceless, since its trace can be included into the filtered pressure term, \bar{p} . With this simplification, most eddy-viscosity models take the following form:

$$\nu_t = (C_m \delta)^2 D_m(\bar{\mathbf{u}}), \quad (3)$$

where C_m is the model constant, δ denotes the subgrid characteristic length, and $D_m(\bar{\mathbf{u}})$ is the model-specific differential operator, with units of frequency. The length scale δ , is the responsible for capturing the effective cut-off length scale, *i.e.*, the spatial scale that separates the resolved turbulent motions, $\bar{\mathbf{u}}$, from the unresolved ones in an LES simulation. Then, the rest of the flow physics, such as the forward/backward scattering, laminar-to-turbulence transitions, 2D flow behavior or presence of walls must be captured by the the differential operator that defines the SGS model, *i.e.*, $D_m(\bar{\mathbf{u}})$.

Over the past decades, advancements in LES have largely centered on calibrating the model constant C_m and improving the accuracy of the model operator $D_m(\overline{\mathbf{u}})$. One of the earliest milestones dates back to the 1960s, when Lilly¹ proposed a method to compute the model constant for the Smagorinsky model², showing excellent performance in simulations of homogeneous isotropic turbulence. However, the Smagorinsky model’s differential operator, $D_m(\overline{\mathbf{u}}) = |\mathbf{S}(\overline{\mathbf{u}})|$, fails to vanish near walls, leading to inaccurate results for wall-bounded flows. Initial attempts to address this limitation relied on wall functions^{3,4}. A significant advancement in this regard came with the dynamic procedure proposed by Germano *et al.*⁵, where the model constant C_m is determined using the Jacobi identity in a least-squares sense, as originally proposed by Lilly⁶. However, this method results in highly fluctuating coefficient fields, often yielding negative values for ν_t , which can introduce numerical instabilities. Consequently, additional techniques such as averaging in homogeneous directions and *ad hoc* clipping of ν_t are typically required. Due to these constraints, the original dynamic procedure is not well-suited for flows in complex geometries that lack homogeneous directions. To overcome these limitations, several alternative approaches have been developed. Ghosal *et al.*⁷ introduced the dynamic localization model, while Meneveau *et al.*⁸ proposed the Lagrangian dynamic model. Along similar lines, Park *et al.*⁹ presented two global dynamic models: one based on the Germano identity¹⁰, and another employing two test filters to enforce a “global equilibrium” between viscous dissipation and subgrid-scale (SGS) dissipation. Later, You and Moin¹¹ proposed a dynamic global approach utilizing only a single test filter. Tejada-Martínez and Jansen^{12,13} adopted an alternative strategy by dynamically calculating the filter-width ratio, which is the only model parameter in the dynamic Smagorinsky model.

Alternatively, models that vanish near solid walls can be developed by constructing appropriate differential operators, $D_m(\overline{\mathbf{u}})$. The first examples thereof are the WALE¹⁴ and the Vreman’s model¹⁵. Later, Nicoud *et al.*¹⁶ introduced the σ -model, while Verstappen proposed the QR -model¹⁷, which was later generalized for anisotropic grids by Rozema *et al.*¹⁸, resulting in the anisotropic minimum dissipation model. This list can be completed with the eddy-viscosity model proposed by Ryu and Iaccarino¹⁹, the family of S3PQR models²⁰ proposed by co-authors of this paper and the vortex-stretching-based eddy-viscosity model²¹. Finally, it is worth mentioning recent physics-constrained machine-learning SGS

closures in which the near-wall scaling is imposed²².

A. Computing the characteristic length scale: a short review

Surprisingly, the computation of the subgrid characteristic length has received comparatively little attention within the LES community, even though it is a fundamental component of any eddy-viscosity model (see Eq.3). Moreover, due to its simplicity and suitability for unstructured meshes, the most commonly adopted definition is the one introduced by Deardorff²³, which defines δ as the cube root of the cell volume. On a Cartesian grid, it reads

$$\delta_{\text{vol}} = (\Delta x \Delta y \Delta z)^{1/3}. \quad (4)$$

Subsequently, Schumann²⁴, Lilly²⁵, and Scotti *et al.*²⁶ proposed various adaptations of δ_{vol} to account for anisotropic grids. It was observed that the Deardorff's length scale provides reasonable accuracy for small anisotropies. However, corrections become necessary for highly anisotropic meshes, such as pancake-like meshes with significantly finer resolution in one spatial direction, which are typically used to capture near-wall turbulence or shear layers. In this regard, Scotti *et al.*²⁶ proposed the following correction:

$$\delta_{\text{Sco}} = f(a_1, a_2) \delta_{\text{vol}}, \quad (5)$$

where $f(a_1, a_2) = \cosh \sqrt{4/27[(\ln a_1)^2 - \ln a_1 \ln a_2 + (\ln a_2)^2]}$ and $a_1 = \Delta x / \Delta z$, $a_2 = \Delta y / \Delta z$, assuming that $\Delta x \leq \Delta z$ and $\Delta y \leq \Delta z$. Later on, Scotti *et al.*²⁷ tested the definition of δ_{Sco} given in Eq. (5) for forced isotropic turbulence using highly anisotropic grids. They compared the theoretical correction factor $f(a_1, a_2)$ with the correction $f_{\text{dyn}}(a_1, a_2)$ obtained by applying the dynamic approach⁵ to $C_m \delta_{\text{vol}} f_{\text{dyn}}(a_1, a_2)$. To do so, they kept C_m constant regardless of the mesh anisotropy. Notice, that the dynamic approach is usually applied to find the model constant, C_m . Their findings indicated that the dynamic model captures the correct trend for pancake-like grids ($a_2 = 1, \Delta x \ll \Delta y = \Delta z$) but fails for pencil-like grids ($a_1 = a_2, \Delta x = \Delta y \ll \Delta z$). A further limitation of the approach proposed by Scotti *et al.*²⁶ (see Eq.5) is that it is applicable only to structured Cartesian grids. To address this, Colosqui and Oberai²⁸ developed an extension suitable for unstructured meshes, assuming that the second-order structure function adheres to the Kolmogorov's hypotheses.

More recent works have focused on the construction²⁹ and performance analysis of different SGS models³⁰ and length scales³¹ on anisotropic grids.

Alternative definitions of the subgrid characteristic length scale, δ , include the L^2 -norm of the 3×3 diagonal tensor

$$\Delta \equiv \text{diag}(\Delta x, \Delta y, \Delta z), \quad (6)$$

divided by $\sqrt{3}$,

$$\delta_{L2} = \sqrt{(\Delta x^2 + \Delta y^2 + \Delta z^2)/3}, \quad (7)$$

and the square root of the harmonic mean of the squares of the grid sizes

$$\delta_{\text{Lapl}} = \sqrt{3/(1/\Delta x^2 + 1/\Delta y^2 + 1/\Delta z^2)}. \quad (8)$$

This quantity is a good estimation of the largest eigenvalue (in absolute value) of the discrete Laplacian. Additionally, in their seminal work on the Detached-Eddy Simulation (DES) method, Spalart *et al.*³² proposed using the maximum dimension of the cell,

$$\delta_{\text{max}} = \max(\Delta x, \Delta y, \Delta z), \quad (9)$$

as a safer and robust definition of δ .

Over the past decade and a half, several subgrid characteristic length scales have been proposed in the context of DES. Chauvet *et al.*³³ were the first to propose making the subgrid length scale, δ , responsive to the local flow topology. In particular, they proposed a new δ that depends on the orientation of the vorticity vector, $\boldsymbol{\omega} = (\omega_x, \omega_y, \omega_z) = \nabla \times \mathbf{u}$,

$$\delta_{\boldsymbol{\omega}} = \sqrt{(\omega_x^2 \Delta y \Delta z + \omega_y^2 \Delta x \Delta z + \omega_z^2 \Delta x \Delta y)/|\boldsymbol{\omega}|^2}. \quad (10)$$

The formulation was later extended to unstructured meshes by Deck³⁴. This definition captures the alignment of the vorticity vector, $\boldsymbol{\omega}$, with the coordinate axis. For example, if $\boldsymbol{\omega} = (0, 0, \omega_z)$, then $\delta_{\boldsymbol{\omega}}$ simplifies to $\sqrt{\Delta x \Delta y}$. This approach was developed to address the issue of excessive subgrid-scale dissipation introduced by δ_{max} in the early stages of shear layers, which are commonly resolved using highly anisotropic grids. In DES simulations, this excess dissipation artificially delays the Kelvin-Helmholtz instabilities by shifting the transition from RANS to LES mode further downstream. Nevertheless, similar to δ_{vol} , the length scale $\delta_{\boldsymbol{\omega}}$ given in Eq.(10) may still be influenced by the smallest grid spacing, which can result in unrealistically low eddy-viscosity values.

To address this issue, Mockett *et al.*³⁵ proposed the following flow-dependent length scale,

$$\tilde{\delta}_\omega = \frac{1}{\sqrt{3}} \max_{n,m=1,\dots,8} |\mathbf{l}_n - \mathbf{l}_m|, \quad (11)$$

where $\mathbf{l} = \boldsymbol{\omega}/|\boldsymbol{\omega}| \times \mathbf{r}_n$ and \mathbf{r}_n ($n = 1, \dots, 8$ for a hexahedral cell) are the locations of the cell vertices. The quantity $\tilde{\delta}_\omega$ represents the diameter of the set of cross-products points, \mathbf{l}_n , divided by $\sqrt{3}$. In the case with $\boldsymbol{\omega} = (0, 0, \omega_z)$, it reduces to $\tilde{\delta}_\omega = \sqrt{(\Delta x^2 + \Delta y^2)/3}$. Hence, it is $\mathcal{O}(\max\{\Delta x, \Delta y\})$ instead of $\delta_{\max} = \Delta z$ (for the common scenario where $\Delta z > \Delta x$ and $\Delta z > \Delta y$) or $\delta_\omega = \sqrt{\Delta x \Delta y}$. Thus, “unlike δ_ω the definition (11) never leads to a strong effect of the smallest grid-spacing on the subgrid-scale δ even though it achieves the desired decrease compared to the δ_{\max} definition in the quasi-2D flow regions treated on strongly anisotropic grids.”³⁶

Later on, Shur *et al.*³⁶ proposed the Shear Layer Adapted (SLA) subgrid length scale

$$\delta_{\text{SLA}} = \tilde{\delta}_\omega F_{KH}(VTM). \quad (12)$$

It is basically a modification of the $\tilde{\delta}_\omega$ given in Eq.(11), where the non-dimensional function $0 \leq F_{KH}(VTM) \leq 1$ is modulated by the Vortex Tilting Measure (VTM) given by

$$VTM = \frac{|(\tilde{\mathbf{S}} \cdot \boldsymbol{\omega}) \times \boldsymbol{\omega}|}{\omega^2 \sqrt{-Q_{\tilde{\mathbf{S}}}}}, \quad (13)$$

where $\tilde{\mathbf{S}}$ represents the traceless component of the rate-of-strain tensor, $\mathbf{S} = 1/2(\nabla \bar{\mathbf{u}} + \nabla \bar{\mathbf{u}}^T)$, *i.e.*, $\tilde{\mathbf{S}} = \mathbf{S} - 1/3\text{tr}(\mathbf{S})\mathbf{I}$. For incompressible flows, where $\text{tr}(\mathbf{S}) = \nabla \cdot \bar{\mathbf{u}} = 0$, it follows that $\tilde{\mathbf{S}} = \mathbf{S}$. Moreover, $Q_{\tilde{\mathbf{S}}}$ denotes the second invariant of the tensor $\tilde{\mathbf{S}}$, given by $Q_{\tilde{\mathbf{S}}} = 1/2(\text{tr}^2(\tilde{\mathbf{S}}) - \text{tr}(\tilde{\mathbf{S}}^2)) = -1/2\text{tr}(\tilde{\mathbf{S}}^2)$. The vortex tilting measure is bounded within the range $0 \leq VTM \leq 1$ and equals zero when the vorticity vector aligns with an eigenvector of \mathbf{S} corresponding to an eigenvalue λ_i , *i.e.*, $\mathbf{S}\boldsymbol{\omega} = \lambda_i\boldsymbol{\omega}$. Thus, the VTM quantifies the extent to which the rate-of-strain tensor tilts the vorticity vector. Finally, the function F_{KH} is designed to trigger the Kelvin-Helmholtz instability in the early stages of a shear layer^{37,38}, while in fully developed 3D turbulent regions, it should recover the original $\tilde{\delta}_\omega$ length scale. In this regard, Shur *et al.*³⁶ proposed several forms for F_{KH} , all satisfying the fundamental constraints: $0 \leq F_{KH}(VTM) \leq 1$, with $F_{KH}(0) = 0$ and $F_{KH}(1) = 1$. Very recent studies evaluating the performance of δ_{SLA} within the framework of DES models can be found in the literature^{39,40}.

More recently, co-authors of the present paper proposed the δ_{lsq} length scale⁴¹

$$\delta_{\text{lsq}} = \sqrt{\frac{\hat{\mathbf{G}}\hat{\mathbf{G}}^T : \mathbf{G}\mathbf{G}^T}{\mathbf{G}\mathbf{G}^T : \mathbf{G}\mathbf{G}^T}}. \quad (14)$$

where $\mathbf{G} \equiv \nabla \bar{\mathbf{u}}$ is the gradient of the resolved velocity and

$$\hat{\mathbf{G}} \equiv \mathbf{G}\Delta, \quad (15)$$

is the gradient in the computational space, *i.e.*, without considering the distances between adjacent nodes, and Δ is the second-order tensor containing the local mesh information given in Eq.(6). The δ_{lsq} length scale given in Eq.(14) follows from the least square minimization between the tensors $\frac{\delta_{\text{lsq}}^2}{12}\mathbf{G}\mathbf{G}^T$ and $\frac{1}{12}\hat{\mathbf{G}}\hat{\mathbf{G}}^T$, respectively. These two tensors correspond to the Clark model⁴², *i.e.*, the leading term in the Taylor-series expansion of the SGS tensor τ , assuming an isotropic filter length equal to δ_{lsq} and an anisotropic filter equal to $\Delta = \text{diag}(\Delta x, \Delta y, \Delta z)$, respectively. This definition of δ has a list of desired properties (locality, boundedness, flow dependence, ...) for LES simulations. Moreover, it has been shown to be a good approach as a grey area mitigation (GAM) technique in the context of DES models particularly for aerodynamic⁴³ and aeroacoustic⁴⁴ simulations. In the latter work⁴⁴, an unstructured vertex-centered edge-based implementation of both δ_ω and $\tilde{\delta}_\omega$ was also presented. For further details on δ_{lsq} , the reader is referred to the original paper⁴¹.

In this study, a new definition of the subgrid characteristic length, δ , is introduced, motivated by the following research question: *can we establish a simple, robust, and easily implementable definition of δ for any type of grid that minimizes the impact of mesh anisotropies on the performance of SGS models?* In doing so, we firstly analyse the entanglement between the numerical discretization and the filtering in LES. This is done in Section II within a finite-volume framework. Next, the new length scale, referred to as the *rational length scale*, is introduced in Section III. Additionally, implementation details are discussed, along with an alternative dissipation-equivalent definition. This new length scale is analysed and numerically tested in Section IV. Finally, relevant results are summarized and conclusions are given.

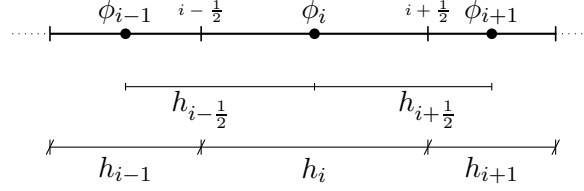


FIG. 1: Example of a one-dimensional mesh.

II. FINITE-VOLUME FILTERING

Let us consider a generic 1D convection-diffusion equation

$$\frac{\partial \phi}{\partial t} + \frac{\partial(u\phi)}{\partial x} = \frac{\partial}{\partial x} \left(\Gamma \frac{\partial \phi}{\partial x} \right), \quad (16)$$

where $u(x, t)$ denotes the advective velocity, $\phi(x, t)$ represents a generic (transported) scalar field and $\Gamma(x)$ is the diffusivity. Within a finite-volume method (FVM), this equation is integrated over a set of non-overlapping volumes. Hence, discrete FVM variables result by applying a box filter with filter width equal to the local grid size, h ,

$$\bar{\phi}(x) = \frac{1}{h} \int_{x-\frac{h}{2}}^{x+\frac{h}{2}} \phi dx. \quad (17)$$

Notice that this filter commutes with differentiation

$$\frac{\partial \bar{\phi}}{\partial x} = \frac{1}{h} \frac{\partial}{\partial x} \int_{x-\frac{h}{2}}^{x+\frac{h}{2}} \phi dx = \frac{1}{h} \int_{x-\frac{h}{2}}^{x+\frac{h}{2}} \frac{\partial \phi}{\partial x} dx = \overline{\frac{\partial \phi}{\partial x}}. \quad (18)$$

Moreover, the standard second-order approximation of the first-derivative at the face is exactly equal to the filtered derivative

$$\left. \frac{\partial \phi}{\partial x} \right|_{i+\frac{1}{2}} \approx \frac{\phi_{i+1} - \phi_i}{h_{i+\frac{1}{2}}} = \frac{1}{h_{i+\frac{1}{2}}} \int_{x_i}^{x_{i+1}} \frac{\partial \phi}{\partial x} dx = \overline{\left. \frac{\partial \phi}{\partial x} \right|_{i+\frac{1}{2}}} \stackrel{\text{Eq.(18)}}{=} \left. \frac{\partial \bar{\phi}}{\partial x} \right|_{i+\frac{1}{2}}. \quad (19)$$

This example corresponds to the 1D non-uniform mesh displayed in Figure 1.

Remark 1 *This result suggests that the actual filter length when computing the face derivative is $h_{i+\frac{1}{2}}$, i.e., the distance between the adjacent nodes i and $i+1$ (see Figure 1).*

Finally, the diffusive term in a FVM framework is approximated as follows

$$\begin{aligned} \left. \frac{\partial}{\partial x} \left(\Gamma \frac{\partial \phi}{\partial x} \right) \right|_i &\approx \frac{1}{h_i} \left(\Gamma \left. \frac{\partial \phi}{\partial x} \right|_{i+\frac{1}{2}} - \Gamma \left. \frac{\partial \phi}{\partial x} \right|_{i-\frac{1}{2}} \right) = \overline{\left. \frac{\partial}{\partial x} \left(\Gamma \frac{\partial \phi}{\partial x} \right) \right|_i} \\ &\approx \frac{1}{h_i} \left(\Gamma_{i+\frac{1}{2}} \frac{\phi_{i+1} - \phi_i}{h_{i+\frac{1}{2}}} - \Gamma_{i-\frac{1}{2}} \frac{\phi_i - \phi_{i-1}}{h_{i-\frac{1}{2}}} \right) = \overline{\left. \frac{\partial}{\partial x} \left(\Gamma \frac{\partial \bar{\phi}}{\partial x} \right) \right|_i}. \end{aligned} \quad (20)$$

In the case of non-constant diffusivity, $\Gamma(x)$, its evaluation at the cell faces can be viewed as box filtering the Γ field, *i.e.*,

$$\Gamma_{i+\frac{1}{2}} \approx \frac{\Gamma_i + \Gamma_{i+1}}{2} \approx \frac{1}{h_{i+\frac{1}{2}}} \int_{x_i}^{x_{i+1}} \Gamma(x) dx = \overline{\Gamma}_{i+\frac{1}{2}}, \quad (21)$$

while using the trapezoidal rule to approximate the integral. Altogether leads to

$$\begin{aligned} \left. \frac{\partial}{\partial x} \left(\Gamma \frac{\partial \phi}{\partial x} \right) \right|_i &\approx \frac{1}{h_i} \left(\frac{\Gamma_{i+1} + \Gamma_i}{2} \frac{\phi_{i+1} - \phi_i}{h_{i+\frac{1}{2}}} - \frac{\Gamma_i + \Gamma_{i-1}}{2} \frac{\phi_i - \phi_{i-1}}{h_{i-\frac{1}{2}}} \right) \\ &= \left. \frac{\partial}{\partial x} \left(\overline{\Gamma} \frac{\partial \phi}{\partial x} \right)^{FV} \right|_i, \end{aligned} \quad (22)$$

where $\overline{(\cdot)}^{FV}$ is the FVM filtering along the cell i whereas the other two filters are applied to the face quantities and their associated filter lengths are $h_{i+\frac{1}{2}}$ and $h_{i-\frac{1}{2}}$, respectively.

Remark 2 *This result suggests that two filtering operations are performed when computing the diffusive term: the calculation of the face derivative (see Eq.19) and the cell-to-face interpolation of the diffusivity coefficient (see Eq.21). Both filtering operators share the same filter length; namely, the distance between the nodes adjacent to the corresponding face.*

Consequently, this suggests that the SGS characteristic length used to compute the eddy viscosity, ν_t , at the face $i+\frac{1}{2}$ should be $h_{i+\frac{1}{2}}$ (see Figure 1). This concept forms the foundation of this paper and is extended to general meshes in the following section.

III. A NEW LENGTH SCALE APPROACH

A. Rational length scale

The formula given in Eq.(22) can be generalized for multiple dimensions (also unstructured grids). Namely, let us first consider the FVM discretization of the diffusive term on an arbitrary mesh

$$\nabla \cdot (\Gamma \nabla \phi) \approx \Omega_c^{-1} \mathbf{M} \Lambda_s \mathbf{G}_h \phi_c. \quad (23)$$

Unless otherwise stated, we follow the FVM notation used in previous works^{45,46}. Namely, in Eq.(23), \mathbf{G}_h denotes the cell-to-face discrete gradient operator,

$$\mathbf{G}_h \equiv \Delta_s^{-1} \mathbf{T}_{cs}, \quad (24)$$

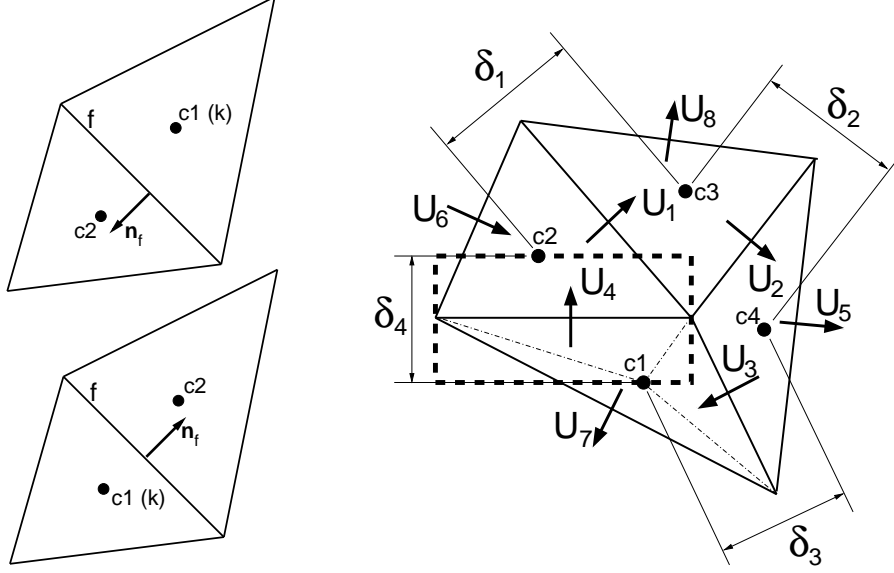


FIG. 2: Left: face normal and neighbor labeling criterion. Right: definition of the volumes, Ω_s , associated with the the face-normal velocities, \mathbf{u}_s . Thick dashed rectangle is the volume associated with the staggered velocity $U_4 = [\mathbf{u}_s]_4$, *i.e.*, $[\Omega_s]_{4,4} = A_4 \delta_4$ where A_4 is the face area and $\delta_4 = |\mathbf{n}_4 \cdot \overrightarrow{c1c2}|$ is the projected distance between adjacent cell centers. Thin dash-dotted lines are placed to illustrate that the sum of volumes is exactly preserved $\text{tr}\Omega_s = \text{tr}\Omega = d\text{tr}\Omega_c$ ($d = 2$ for 2D and $d = 3$ for 3D) regardless of the location of the cell nodes.

where T_{cs} is the cell-to-face oriented incidence matrix. The sub-index h is used here to stress that G_h is a discrete operator and to avoid confusion with the gradient tensor of the resolved velocity, $\mathsf{G} \equiv \nabla \bar{\mathbf{u}}$. Notice that T_{cs} has two non-zero elements per row (a $+1$ and a -1 corresponding to the cells adjacent to a face), whereas the face-to-cell incidence matrix, T_{sc} , corresponds to its transpose, $\mathsf{T}_{sc} = \mathsf{T}_{cs}^T$. For example, for the mesh with 4 control volumes and 8 faces shown in Figure 2 (right), the latter reads

$$\mathsf{T}_{sc} = \mathsf{T}_{cs}^T = \begin{pmatrix} 0 & 0 & -1 & +1 & 0 & 0 & +1 & 0 \\ +1 & 0 & 0 & -1 & 0 & -1 & 0 & 0 \\ -1 & +1 & 0 & 0 & 0 & 0 & 0 & +1 \\ 0 & -1 & +1 & 0 & +1 & 0 & 0 & 0 \end{pmatrix}. \quad (25)$$

Moreover, the diagonal matrix Δ_s contains the projected distances between adjacent cell centers (see δ_i with $i = \{1, \dots, 4\}$ in Figure 2). Therefore, the formula in Eq.(23) corresponds to the standard second-order gradient calculation, which, in 1D, leads to the result given in

Eq.(19). Notice that subindices c and s refers to whether quantities are located at the cell nodes or staggered at the faces.

Then, the integrated divergence operator is defined as follows

$$\mathbf{M} \equiv -\mathbf{G}_h^T \Omega_s \stackrel{(24)}{=} -\mathbf{T}_{cs}^T \Delta_s^{-1} \Omega_s = -\mathbf{T}_{cs}^T \mathbf{A}_s. \quad (26)$$

In this way, the duality between the gradient and the divergence operators is preserved at discrete level. Notice that $\Omega_s \equiv \Delta_s \mathbf{A}_s$ is a diagonal matrix containing the staggered volumes whereas \mathbf{A}_s is a diagonal matrix containing the corresponding surface areas. Finally, Ω_c and Λ_s are diagonal matrices containing the cell volumes and the diffusivities associated with the faces, respectively.

Then, combining Eqs.(23), (24) and (26), we obtain

$$\nabla \cdot (\Gamma \nabla \phi) \approx -\Omega_c^{-1} \underbrace{\mathbf{T}_{cs}^T \mathbf{A}_s}_{-\mathbf{M}} \Lambda_s \underbrace{\Delta_s^{-1} \mathbf{T}_{cs}}_{\mathbf{G}_h} \phi_c = -\Omega_c^{-1} \underbrace{\mathbf{T}_{cs}^T \Delta_s^{-1} \Omega_s}_{-\mathbf{M}} \Lambda_s \underbrace{\Delta_s^{-1} \mathbf{T}_{cs}}_{\mathbf{G}_h} \phi_c. \quad (27)$$

Here, we can neatly identify the filter lengths associated with the box filtering applied to the gradient (see Eq. 19); that is, the matrix Δ_s that contains the projected distances between the adjacent cell centers.

Hence, if diffusivities Λ_s are replaced by $\tilde{\Lambda}_s$, which is a diagonal matrix containing the inverses of the characteristic relaxation times, multiplied by their associated length scales, it reads

$$\Lambda_s \equiv \Delta_s \tilde{\Lambda}_s \Delta_s. \quad (28)$$

Plugging this into Eq.(27) leads to

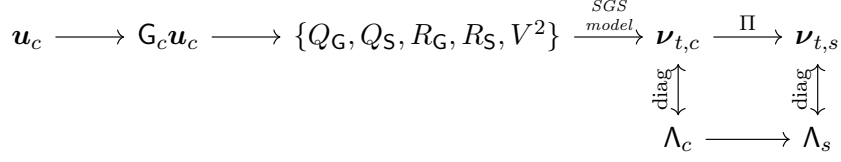
$$\mathbf{M}(\Gamma \mathbf{G}_h \phi) \approx -\Omega_c^{-1} \mathbf{T}_{cs}^T \Omega_s \tilde{\Lambda}_s \mathbf{T}_{cs} \phi_c. \quad (29)$$

Hence, we are computing the gradient (and its transpose) without distances, *i.e.*, in the so-called computational space.

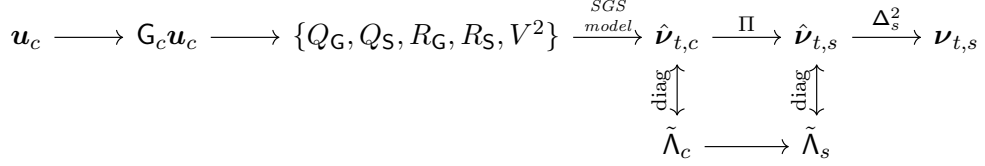
An alternative interpretation is the following: going back to the original formula given in Eq.(23)

$$\nabla \cdot (\Gamma \nabla \phi) \approx \Omega_c^{-1} \mathbf{M} \Lambda_s \mathbf{G}_h \phi_c \stackrel{(28)}{=} \Omega_c^{-1} \mathbf{M} \Delta_s^2 \tilde{\Lambda}_s \mathbf{G}_h \phi_c. \quad (30)$$

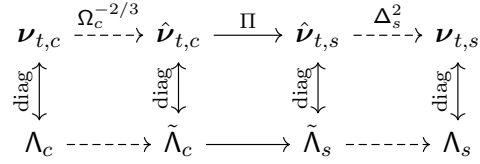
Here, it is very easy to identify the analogy with the formula given in Eq.(22). This naturally leads to a definition of the length scale for SGS models, Δ_s , which is computed directly at the



(a) Standard flowchart to computed the eddy-viscosity at the cell faces, $\boldsymbol{\nu}_{t,s}$.



(b) Modified flowchart to computed the eddy-viscosity at the cell faces, $\boldsymbol{\nu}_{t,s}$.



(c) Flowchart for the implementation of the δ_{rls} . Dashed lines represent the modifications required respect to the standard flowchart.

FIG. 3: Flowcharts to compute the eddy-viscosity at the cell faces, $\boldsymbol{\nu}_{t,s}$.

faces and corresponds to the distance between adjacent cell centers (see δ_i with $i = \{1, \dots, 4\}$ in Figure 2). Hereafter, this new length scale is denoted by δ_{rls} and referred to as *rational length scale*, as it naturally arises from the entanglement between numerical discretization and the LES filtering.

B. Practical implementation and an alternative definition

The newly proposed length scale, δ_{rls} , is directly computed at the faces as the distance between adjacent cell centers. However, in virtually all codes, the turbulent viscosity is computed at cell centers and then interpolated to the faces. The overall process is depicted in the flowchart displayed in Figure 3a. Namely, firstly the gradient of the resolved velocity field, $\mathbf{G}_c \mathbf{u}_c$ is computed at the cells; then, the eddy-viscosity, $\boldsymbol{\nu}_{t,c}$, is calculated at the cells based on the five basic invariants of the velocity gradient tensor, as virtually all existing models can be reformulated as combinations of these invariants²⁰. Then, $\boldsymbol{\nu}_{t,c}$ is interpolated

to the faces, *i.e.*, $\boldsymbol{\nu}_{t,s} = \Pi \boldsymbol{\nu}_{t,c}$, where Π is a cell-to-face interpolation defined as

$$\Pi \equiv \frac{1}{2} |\mathbb{T}_{cs}|, \quad (31)$$

which is the cell-to-face midpoint interpolation. In our case, we need to slightly modify the flowchart as shown in Figure 3b. Specifically, the only required modifications are indicated by dashed lines in the flowchart displayed in Figure 3c. Thus, the two changes are basically two geometrical re-scalings. Firstly, if we assume that δ_{vol} is used in the calculation of $\boldsymbol{\nu}_{t,c}$, we need to divide it by $\Omega_c^{2/3}$, which is the diagonal matrix that contains the cell volumes, *i.e.*, δ_{vol} at cell i is given by $[\Omega_c^{1/3}]_{i,i}$. In this way, we obtain a pseudo-eddy-viscosity, $\hat{\boldsymbol{\nu}}_{t,c}$, computed without any length scale and thus having units of inverse time. Then, a second re-scaling is required to compute the actual eddy-viscosity at the faces, $\boldsymbol{\nu}_{t,s}$, from $\hat{\boldsymbol{\nu}}_{t,s}$, *i.e.*, $\boldsymbol{\nu}_{t,s} \equiv \Delta_s^2 \hat{\boldsymbol{\nu}}_{t,s}$.

Therefore, from an implementation and conceptual point-of-view, the new approach δ_{rls} is completely different from all previous definitions of δ since it is directly computed at the faces. Although the required code modifications are minimal, it may be of interest to compute a length scale at the cells that provides the same dissipation. Namely, it can be shown that the local dissipation of the viscous term, with constant viscosity, is given by

$$\nu \mathbf{G} : \mathbf{G} = \nu \text{tr}(\mathbf{G}\mathbf{G}^T). \quad (32)$$

If we replace ν by ν_t , we can obtain a very accurate estimation of the local dissipation introduced by an eddy-viscosity model. Furthermore, in the new approach we also need to replace ν_t and \mathbf{G} by $\hat{\nu}_t$ and $\hat{\mathbf{G}}$ (see Eq.15), respectively, leading to

$$\hat{\nu}_t \hat{\mathbf{G}} : \hat{\mathbf{G}} = \hat{\nu}_t \text{tr}(\hat{\mathbf{G}}\hat{\mathbf{G}}^T). \quad (33)$$

Then, we can compute an equivalent filter length, $\tilde{\delta}_{\text{rls}}$, that leads to the same local dissipation, *i.e.*,

$$\tilde{\delta}_{\text{rls}}^2 \hat{\nu}_t \hat{\mathbf{G}} : \hat{\mathbf{G}} = \hat{\nu}_t \hat{\mathbf{G}} : \hat{\mathbf{G}} \quad \Longrightarrow \quad \boxed{\tilde{\delta}_{\text{rls}} = \sqrt{\frac{\hat{\mathbf{G}} : \hat{\mathbf{G}}}{\hat{\mathbf{G}} : \hat{\mathbf{G}}}} = \sqrt{\frac{\text{tr}(\hat{\mathbf{G}}\hat{\mathbf{G}}^T)}{\text{tr}(\hat{\mathbf{G}}\hat{\mathbf{G}}^T)}}} \quad (34)$$

Notice that $P_{\mathbf{G}\mathbf{G}^T} = \text{tr}(\mathbf{G}\mathbf{G}^T)$ is the first invariant of the symmetric tensor $\mathbf{G}\mathbf{G}^T$.

Property	Relevance	Description
P1	must	positive ($\delta > 0$), local and frame invariant
P2	must	bounded, <i>e.g.</i> , for Cartesian mesh with $\Delta x \leq \Delta y \leq \Delta z$, $\Delta x \leq \delta \leq \Delta z$
P3	optional	sensitive to the local flow field, \mathbf{G}
P4	practical	applicable to unstructured meshes
P5	practical	length scale is directly computed at the cell faces
P6	efficient	computational cost
P7	efficient	memory footprint

TABLE I: List of potential properties of the subgrid characteristic length, δ .

	δ_{vol}	δ_{Sco}	δ_{max}	δ_{L2}	δ_{Lapl}	δ_{ω}	$\tilde{\delta}_{\omega}$	δ_{SLA}	δ_{lsq}	δ_{rls}	$\tilde{\delta}_{\text{rls}}$
Formula	Eq.(4)	Eq.(5)	Eq.(9)	Eq.(7)	Eq.(8)	Eq.(10)	Eq.(11)	Eq.(12)	Eq.(14)	Eq.(30)	Eq.(34)
P1	Yes	Yes	Yes	Yes	Yes	Yes	Yes	Yes	Yes	Yes	Yes
P2	Yes	Yes	Yes	Yes	Yes	Yes	Yes	No	Yes	Yes	Yes
P3	No	No	No	No	No	Yes	Yes	Yes	Yes	No ^c	Yes
P4	Yes	No	No ^a	No	No ^a	No ^b	Yes	Yes	Yes	Yes	Yes
P5	No	No	No	No	No	No	No	No	No	Yes	No
P6	+	+	+	+	+	++	+++	++++	+++	+	+++
P7	+	+	+	+	+	++	++	+++	+++	+	+++

TABLE II: Properties of different definitions of the subgrid characteristic length, δ . See Table I for a short description of these properties. ^a Possible with some adaptations, ^b Deck³⁴ proposed a generalization for unstructured meshes. ^c δ_{rls} is computed at the faces independently of the local flow field, however, its effect ultimately depends on it.

IV. ANALYSIS OF THE NEW APPROACH AND NUMERICAL TESTS

A. Fundamental properties

Starting with the classical Smagorinsky model², numerous eddy-viscosity models (see Eq.2) have been developed over the past decades⁴⁷. The definition of ν_t in Eq.(3) serves as

a general framework for most of these models, requiring a subgrid characteristic length, δ , which is typically related to the local grid size. In isotropic grids, δ corresponds to the mesh size, *i.e.*, $\delta = \Delta x = \Delta y = \Delta z$. However, there is still no consensus on how to define δ for (highly) anisotropic or unstructured grids. Despite its potential inaccuracies in certain cases, more than four decades later, the approach introduced by Deardorff²³, *i.e.*, using the cube root of the cell volume (see Eq.4), remains the most widely used method in both academia and industry.

Section I provides an overview of alternative approaches for computing δ , which are classified in Table II according to a set of desirable criteria (see Table I) grounded in physical reasoning, numerical stability, and practical implementation. The first criterion, labeled as **P1**, requires the length scale to be both positive and local. Although negative values of ν_t may be justified from a physical perspective due to the backscatter phenomenon, from a numerical standpoint, enforcing $\nu_t \geq 0$ is usually preferred to ensure simulation stability. Additionally, to preserve Galilean invariance, a fundamental physical principle, flow-dependent definitions of δ (see property **P3** below) are formulated using invariants of the velocity gradient, $\mathbf{G} \equiv \nabla \bar{\mathbf{u}}$. This approach guarantees locality, which is particularly beneficial for applications involving complex flows. The second property [**P2**] ensures that δ remains properly bounded. Specifically, for a structured Cartesian mesh where $\Delta x \leq \Delta y \leq \Delta z$, we require that $\Delta x \leq \delta \leq \Delta z$. All length scales presented in Table II satisfy properties **P1** and **P2**, except the δ_{SLA} that can eventually lead to values of δ smaller than the smallest grid size. The third property [**P3**] classifies the approaches for computing δ into two categories: into purely geometry-based definitions and those that incorporate flow-dependent information, particularly the velocity gradient, \mathbf{G} .

Examples of the former category have been introduced in the context of DES by Chauvet *et al.*³³ (see the definition of δ_{ω} in Eq.10), Mockett *et al.*³⁵ (see $\tilde{\delta}_{\omega}$ in Eq.11), the modified version δ_{SLA} proposed by Shure *et al.*³⁶ (see Eq.12) and the definition of δ_{lsq} proposed by co-authors of this paper⁴¹ (see Eq.14). This list is further expanded with $\tilde{\delta}_{\text{rls}}$, given in Eq.(34). Notice that δ_{rls} , given in Eq.(30), is computed at the faces independently of the local flow field, however, its effect ultimately depends on it, as remarked in Table II.

The last four properties of the subgrid characteristic length scale, δ , are mainly of practical significance. Property **P4** refers to its applicability to unstructured meshes. In this

regard, all flow-dependent definitions of δ , satisfy this property, including the newly proposed $\tilde{\delta}_{\text{rls}}$ length scale. However, among the definitions of δ that are independent of the local flow, only the Deardorff's approach²³ and the newly proposed length scale δ_{rls} can be directly applied to unstructured grids. Additionally, δ_{rls} is the only length scale computed directly at the faces, as stated by property **P5**. All other length scales are first computed at the cell and then interpolated to the faces. This interpolation can, in fact, be seen as an unnecessary cell-to-face (box) filtering operation (see Eq.21). Finally, it is also important that the definition of δ is well-conditioned and computationally efficient, as stated in property **P6**. Moreover, a low memory footprint (property **P7**) is another key feature that makes LES simulations more affordable on modern HPC systems. However, flow-dependent formulations can pose challenges in these last two properties, often demanding significantly higher computational resources. Moreover, they must be carefully implemented to avoid numerical issues, particularly when dealing with indeterminate forms such as 0/0. In this regard, the newly proposed length scale δ_{rls} is virtually costless, both in terms of computational cost and memory, as it only needs to be computed once at the faces, independently of the local flow field.

B. Analysis of simple flows

To get a better understanding of δ_{rls} and $\tilde{\delta}_{\text{rls}}$, we firstly analyze several special cases. Firstly, for isotropic meshes they reduce to $\delta = \Delta x = \Delta y = \Delta z$ regardless of the flow topology, whereas for anisotropic grids they always remain well-bounded (property **P2**). Secondly, for pure rotation flows, *i.e.*, $\mathbf{S} = \mathbf{0}$ and $\mathbf{G} = \Omega$, $\tilde{\delta}_{\text{rls}}$ leads to

$$\tilde{\delta}_{\text{rls}} = \frac{\omega_x^2(\Delta y + \Delta z) + \omega_y^2(\Delta x + \Delta z) + \omega_z^2(\Delta x + \Delta y)}{2|\boldsymbol{\omega}|^2}, \quad (35)$$

which resembles the definition of $\delta_{\boldsymbol{\omega}}$ proposed by Chauvet *et al.*³³ given in Eq. (10). Actually, similarly to the definition of $\tilde{\delta}_{\boldsymbol{\omega}}$ proposed by Mockett *et al.*³⁵ given in Eq. (11), $\tilde{\delta}_{\text{rls}}$ (also δ_{rls}) is $\mathcal{O}(\max\{\Delta x, \Delta y\})$ instead of $\delta_{\boldsymbol{\omega}} = \sqrt{\Delta x \Delta y}$ in the case where $\boldsymbol{\omega} = (0, 0, \omega_z)$. Therefore, it also avoids strong effects of the smallest grid-spacing in the initial part of a shear layer.

Finally, results obtained for the following 2D mesh and flow topology

$$\Delta = \begin{pmatrix} \Delta x & 0 \\ 0 & \Delta y \end{pmatrix} = \begin{pmatrix} \beta & 0 \\ 0 & \beta^{-1} \end{pmatrix}, \quad \mathbf{G} = \begin{pmatrix} \partial_x u & \partial_y u \\ \partial_x v & \partial_y v \end{pmatrix} = \begin{pmatrix} 0 & 1 \\ 1 - 2\omega & 0 \end{pmatrix}, \quad (36)$$

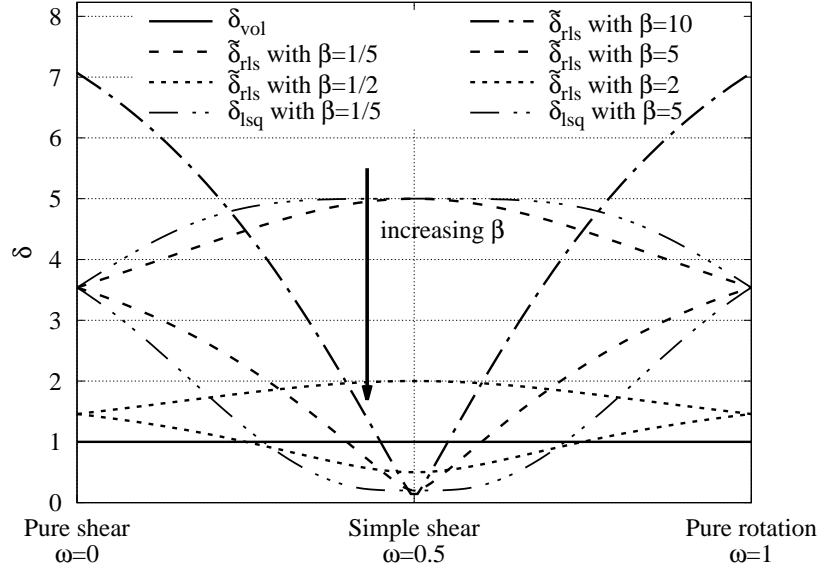


FIG. 4: Comparison between $\tilde{\delta}_{\text{rls}}$ and δ_{vol} for the simple 2D flow defined in Eq.(36) with different values of $\beta = \{1/5, 1/2, 2, 5, 10\}$.

are displayed in Figure 4. Since the control volume is fixed to unity, the Deardorff length scale, δ_{vol} , remains constant at 1, independent of the value of β . On the other hand, values of ω in Figure 4 range from a pure shear flow ($\omega = 0$) to a simple shear flow ($\omega = 1/2$), to a pure rotating flow ($\omega = 1$). For the two limiting situations $\tilde{\delta}_{\text{rls}} = \sqrt{(\beta^2 + \beta^{-2})/2}$ whereas for $\omega = 1/2$ it reads $\tilde{\delta}_{\text{rls}} = \beta^{-1}$. Recalling that, in this particular case, $\Delta x = \beta$ and $\Delta y = \beta^{-1}$, $\tilde{\delta}_{\text{rls}} = \sqrt{(\Delta x^2 + \Delta y^2)/2}$ for $\omega = 0$ (pure shear) and $\omega = 1$ (pure rotation), whereas $\tilde{\delta}_{\text{rls}} = \Delta y$ for the simple shear flow with $\omega = 1/2$. The latter case closely corresponds to the typical quasi-2D, grid-aligned flow observed in the initial region of a shear layer. As expected, the computed $\tilde{\delta}_{\text{rls}}$ (also the δ_{rls} length scale) matches the grid size in the direction perpendicular to the shear layer. The purely rotational flow ($\omega = 1$) is a special case of Eq. (35), where $\omega_x = \omega_y = 0$ and $\omega_z = 1$. It is worth noting that Figure 4 also includes results for the δ_{lsq} length scale⁴¹, defined in Eq. (14). This length scale yields the same values as $\tilde{\delta}_{\text{rls}}$ for pure shear ($\omega = 0$), simple shear flow ($\omega = 1/2$), and pure rotation ($\omega = 1$). Differences arise in the transitions between these regimes: specifically, δ_{lsq} exhibits a wider plateau around $\omega = 1/2$, whereas δ_{rls} transitions more rapidly. Similar behavior is observed for other values of β , with the differences between δ_{lsq} and $\tilde{\delta}_{\text{rls}}$ remaining qualitatively the same.

To gain deeper insight into the impact of mesh anisotropy on various δ definitions, let

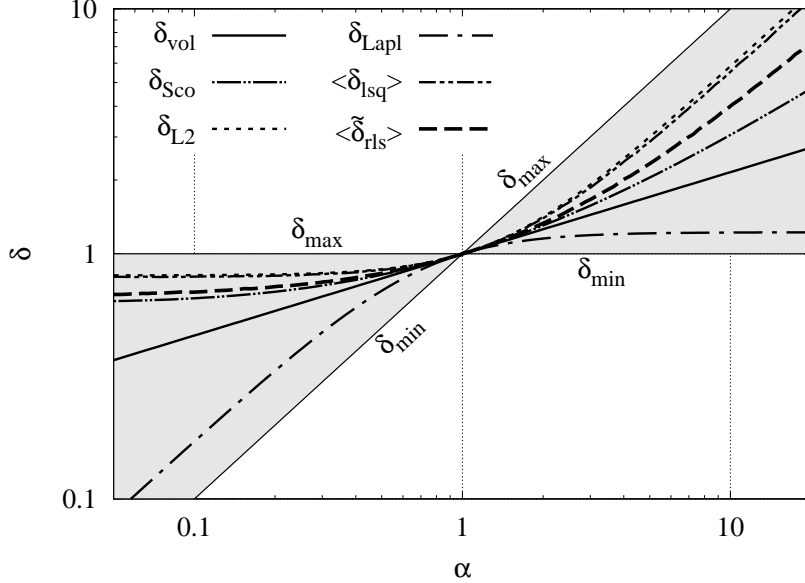


FIG. 5: Scaling of different definitions of δ for a Cartesian mesh with $\Delta x = \Delta y = 1$ and $\Delta z = \alpha$. Average results of δ_{lsq} and $\tilde{\delta}_{\text{rls}}$ have been obtained from a large enough sample of random traceless velocity gradient tensors.

us consider a Cartesian mesh with $\Delta x = \Delta y = 1$ and $\Delta z = \alpha$. In this case, the geometry-dependent definitions of δ result in

$$\begin{aligned} \delta_{\text{vol}} &= \alpha^{1/3}, & \delta_{\text{Sco}} &= f(\min(\alpha, \alpha^{-1}), \min(1, \alpha^{-1}))\alpha^{1/3}, \\ \delta_{\text{max}} &= \max(1, \alpha), & \delta_{\text{L2}} &= \sqrt{\frac{2 + \alpha^2}{3}}, & \delta_{\text{Lapl}} &= \sqrt{\frac{3\alpha^2}{2\alpha^2 + 1}}. \end{aligned} \quad (37)$$

where $f(a_1, a_2)$ is the correcting function given in Eq.(5). These functions are displayed in Figure 5 using a log-log scale. Values of $\alpha > 1$ correspond to pencil-like meshes ($\Delta x = \Delta y \ll \Delta z$) whereas values of $\alpha < 1$ correspond to pancake-like meshes ($\Delta x \ll \Delta y = \Delta z$). The averaged values of δ_{lsq} and $\tilde{\delta}_{\text{rls}}$ are also displayed; they have been obtained from a sufficiently large sample of random traceless velocity gradient tensors, \mathbf{G} . Among all the geometry-dependent definitions, the δ_{L2} given in Eq.(7) is by far the closest to $\langle \delta_{\text{lsq}} \rangle$ for the mesh considered here. In fact, for simple flow configurations such as pure shear or pure rotation, δ_{lsq} simplifies to δ_{L2} . On the other hand, $\tilde{\delta}_{\text{rls}}$ falls between δ_{L2} and the correction proposed by Scotti *et al.*²⁶ (see Eq.5). Finally, δ_{Lapl} is the only definition that predicts values of δ smaller than the classical Deardorff length scale, δ_{vol} .

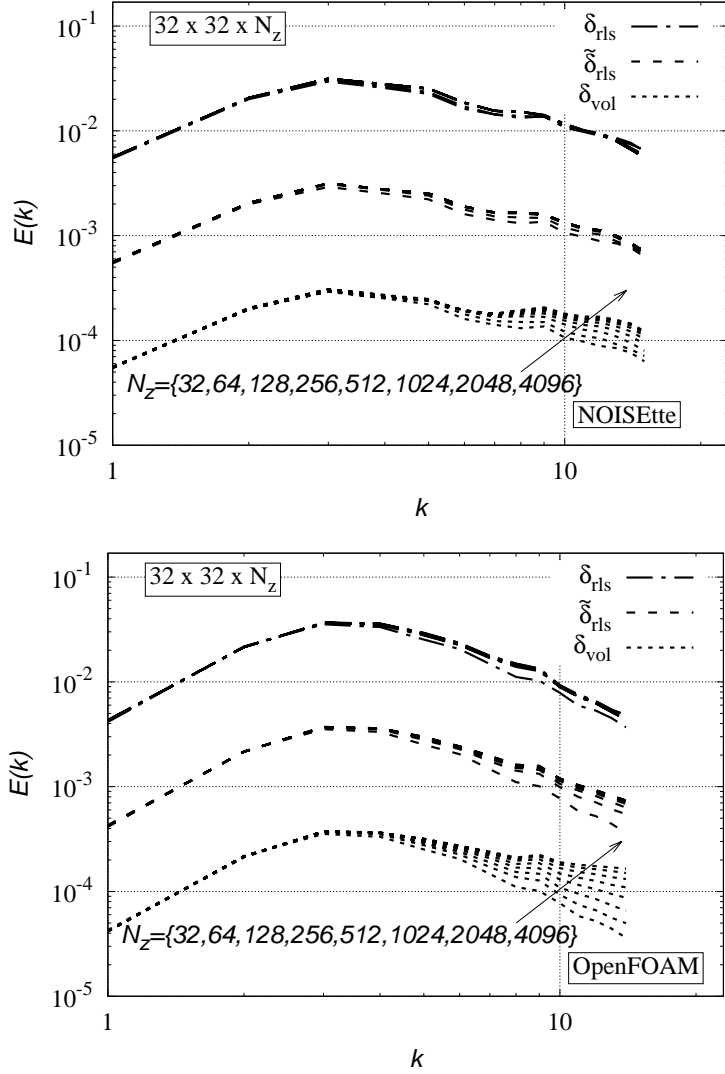


FIG. 6: Energy spectra for decaying isotropic turbulence corresponding to the Comte-Bellot and Corrsin experimental set-up⁴⁸. LES results were obtained using the Smagorinsky model on a set of anisotropic meshes with pancake-like control volumes, employing two different codes: the in-house NOISEtte code (top) and OpenFOAM (bottom). Results obtained with the novel definitions of δ_{rls} and $\tilde{\delta}_{\text{rls}}$ respectively proposed in Eqs. (30) and (34) are compared with the classical definition proposed by Deardorff, given in Eq. (4). For clarity, the results obtained with $\tilde{\delta}_{\text{rls}}$ and δ_{vol} are shifted down one and two decades, respectively.

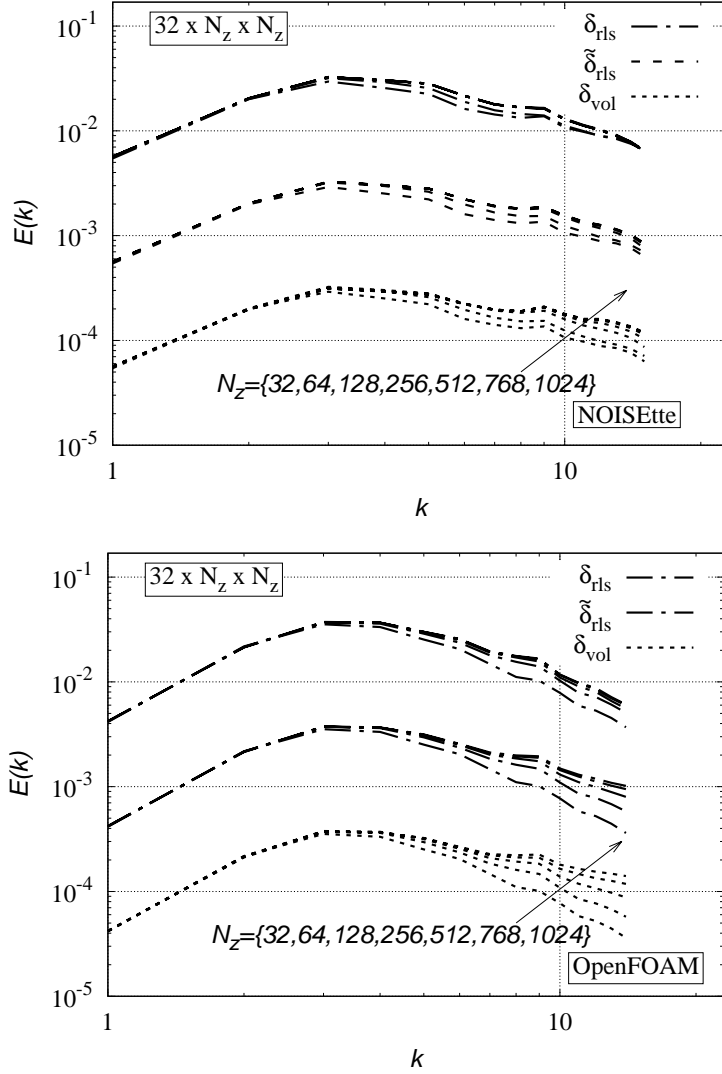


FIG. 7: Same as Figure 6 but for pencil-like meshes.

C. Isotropic turbulence on anisotropic grids

Finally, the numerical simulation of decaying isotropic turbulence is chosen to test the novel definitions of the subgrid characteristic length scale, δ_{rls} and $\tilde{\delta}_{\text{rls}}$, proposed in Eqs. (30) and (34), respectively. The configuration corresponds to the classical experiment of Comte-Bellot and Corrsin⁴⁸ (hereafter denoted as CBC) using the grid turbulence with a size of $M = 5.08\text{cm}$ and a free-stream velocity $U_0 = 10\text{m/s}$. The Taylor micro-scale Reynolds number at $tU_0/M = 42$ (initial state) is $Re_\lambda = u_{\text{rms}}\lambda/\nu = 71.6$ with $u_{\text{rms}} = 22.2\text{cm/s}$ and decreases to 60.6 at $tU_0/M = 171$ (third stage).

The results are non-dimensionalized with the reference length $L_{\text{ref}} = 11M/(2\pi)$ and

reference velocity $u_{ref} = \sqrt{3/2}u_{rms}|_{tU_0/M=42}$. The energy spectrum of the initial field at $tU_0/M = 42$ matches the CBC experimental data. All subsequent results are presented at $tU_0/M = 98$, which corresponds to the second stage of the CBC experimental data.

Simulations are carried out using two different codes: namely, the in-house NOISEtte code^{49,50} and OpenFOAM. NOISEtte is based on high-accuracy Edge-Based Reconstruction (EBR) finite-volume schemes⁵¹. On translationally invariant (structured) meshes, EBR schemes are equivalent to high-order finite-difference methods, reaching up to sixth-order accuracy. For LES simulations, central-difference EBR4 was used to minimize artificial numerical dissipation. On the other hand, OpenFOAM simulations were performed using OpenFOAM v2312, with appropriate modifications to the *decayIsoTurb* tutorial. The solver used for all length scales was *pimpleFoam*, employing two internal correctors and a single outer corrector. The selected time integration scheme was the implicit second-order "Backward" scheme, with a fixed time step ensuring $CFL < 1$ for cases up to $32 \times 32 \times 1024$, while a more stringent condition of $CFL < 0.5$ was applied for finer meshes. The linear scheme was used for the gradient, divergence, and Laplacian operators to minimize numerical diffusion. The setup for these cases, along with all necessary files to reproduce the obtained results in OpenFOAM (including modifications to the *TurbulenceModel* library) are publicly available⁵². For both codes, the initial velocity fields were obtained by interpolating a velocity field on a $64 \times 64 \times 64$ with an energy spectrum corresponding to the CBC initial spectrum.

LES results have been carried out for a set of (artificially) stretched meshes using the Smagorinsky model with constant equal to $C_S = 0.17$ (NOISEtte) and $C_S = 0.21$ (OpenFOAM). These constants have been calibrated for the $32 \times 32 \times 32$ mesh and kept constant for the rest of simulations. In particular, results for pancake-like meshes with dimensions $32 \times 32 \times N_z$, where $N_z = \{32, 64, 128, 256, 512, 1024, 2048, 4096\}$, are presented in Figure 6. As expected, when using Deardorff's classical definition (see Eq.4), the results tend to diverge as N_z increases. This occurs because δ_{vol} approaches zero with increasing N_z , effectively disabling the SGS model. In contrast, the newly proposed δ_{rls} and $\tilde{\delta}_{rls}$ avoid this issue, and the results rapidly converge for larger values of N_z . These trends, observed for both codes, suggest that they effectively reduce the influence of mesh anisotropies on the SGS model performance.

A similar trend is observed in Figure 7 for pencil-like meshes composed of $32 \times N_z \times N_z$ grid cells, where $N_z = \{32, 64, 128, 256, 512, 768, 1024\}$. In this case, δ_{vol} scales as $\mathcal{O}(\Delta z^{4/3})$ compared to the $\mathcal{O}(\Delta z^{2/3})$ scaling for the pancake-like meshes, causing the eddy-viscosity model (see Eq.3) to switch off even more quickly for increasing values of N_z . Moreover, in this case, the numerical artifact affects a broader range of wavenumbers, whereas for pancake-like meshes, the impact is mostly confined to the smallest resolved scales (see Figure 6). In contrast, LES results obtained with δ_{rls} and $\tilde{\delta}_{\text{rls}}$ show convergence as N_z increases. However, more noticeable variations are observed for the first three mesh resolutions, *i.e.*, $N_z = \{32, 64, 128\}$, compared to the pancake-like cases. This slower convergence may be due to the fact that, in pencil-like meshes, finer resolution is achieved in two spatial directions instead of one, meaning that more physical scales are being resolved. As a result, the SGS model plays a reduced role, and the observed differences are likely related to the natural convergence due to grid refinement. In any case, the newly proposed subgrid characteristic length scales, δ_{rls} and $\tilde{\delta}_{\text{rls}}$, significantly mitigate the artificial effects caused by mesh anisotropies and ensure more consistent convergence behavior compared to the classical Deardorff approach.

To gain deeper insight into the impact of mesh anisotropies on different definitions of δ , two key physical quantities have been analyzed: the resolved kinetic energy and the resolved enstrophy. Reference values are computed by integrating the second stage of the CBC data⁴⁸ up to the cut-off length scale defined by our LES resolution. This leads to a reference value for the resolved turbulent kinetic energy of approximately 0.39, which corresponds to around 67% of the total turbulent kinetic energy. Results displayed in Figures 8, 9 and 10 have been obtained with the same pancake-like meshes, *i.e.*, $32 \times 32 \times N_z$ grid cells where $N_z = \{32, 64, 128, 256, 512, 1024, 2048, 4096\}$. In this case, we have firstly compared definitions that depend solely on the mesh geometry and not on the flow topology (see Figure 8). This analysis was performed exclusively for NOISEtte. Namely, in addition to the new approach, δ_{rls} , and the Deardorff length scale, δ_{vol} , two other definitions have been tested: the definition proposed by Scotti *et al.*²⁶, δ_{SCO} , given in Eq. (5), and $\delta_{\text{min}} = \min(\Delta x, \Delta y, \Delta z)$, which establishes a lower bound for the other definitions. It is important to note that δ_{SCO} is chosen for this comparison because, among all the definitions reviewed in Section I that rely solely on the geometrical properties of the mesh (see property **P3** in Table II), it is the length scale that yields the best results. As expected, the results obtained with δ_{vol} get closer and closer to those obtained with δ_{min} as N_z increases, since in both cases, the SGS

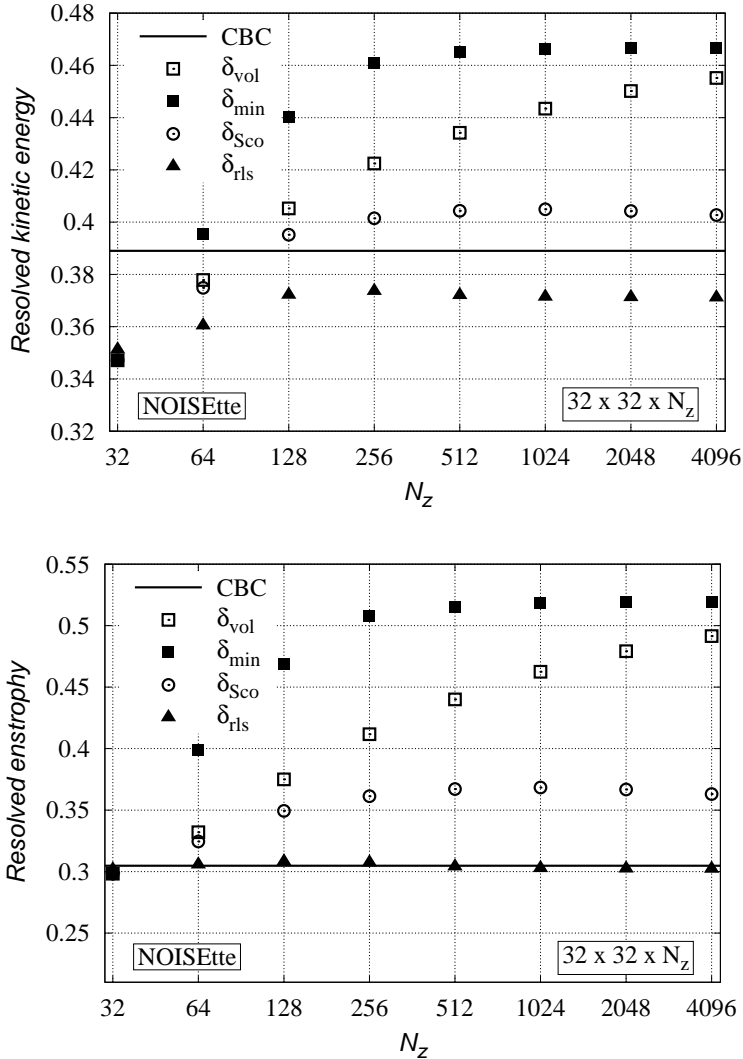


FIG. 8: Resolved kinetic energy (top) and enstrophy (bottom) as a function of the number of grid points, N_z , for decaying isotropic turbulence corresponding to the experiment of Comte-Bellot and Corrsin⁴⁸. LES results have been obtained using the Smagorinsky model for a set of anisotropic meshes with pancake-like control volumes, *i.e.*, $32 \times 32 \times N_z$. Results correspond to definitions of δ that depend solely on the mesh geometry: δ_{vol} , δ_{min} , δ_{Sco} and the novel definition δ_{rls} .

model tends to switch off. Remarkably, the new definition δ_{rls} clearly outperforms other ones, including Scotti's length scale, δ_{Sco} . As explained in Section I, this definition of δ was proposed as a correction of the Deardorff definition, δ_{vol} , for anisotropic meshes with the assumption of an isotropic turbulent regime. Therefore, it is not surprising that δ_{Sco} behaves

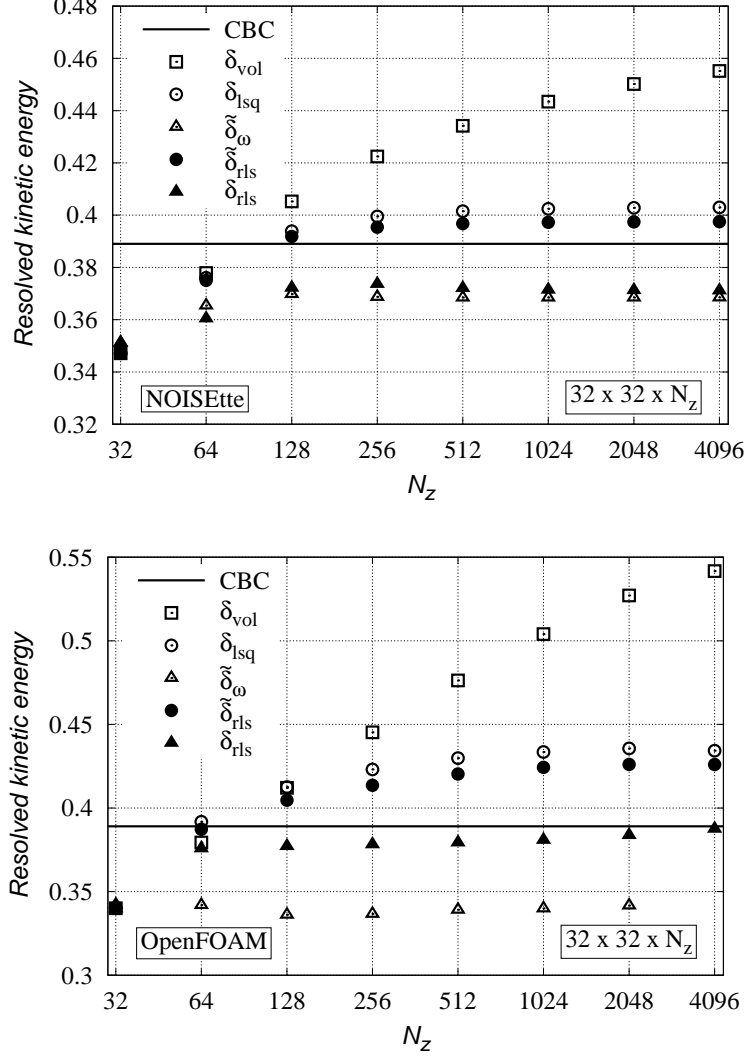


FIG. 9: Same as Figure 8 (top). In this case, results were obtained with two different codes: the in-house NOISEtte code (top) and OpenFOAM (bottom). Moreover, in addition to δ_{vol} and δ_{rls} (also shown in Figure 8), results include definitions of δ that depend on the flow topology: δ_{lsq} , $\tilde{\delta}_{\omega}$, and the newly proposed definition, $\tilde{\delta}_{rls}$.

very robustly for a simulation of decaying homogeneous isotropic turbulence. Furthermore, it is very remarkable the robustness of the new definition in the enstrophy results displayed in Figure 8 (bottom). Notice that enstrophy, which is the L2-norm, $\mathcal{E} \equiv \|\boldsymbol{\omega}\|^2 = \int_{\Omega} |\boldsymbol{\omega}|^2 d\Omega$, of the vorticity vector, $\boldsymbol{\omega} \equiv \nabla \times \mathbf{u}$, reads $\mathcal{E}_k = k^2 E_k$ in Fourier space. Therefore, enstrophy magnifies errors in the tail of the kinetic energy spectrum which is a key parameter in the assessment of SGS models.

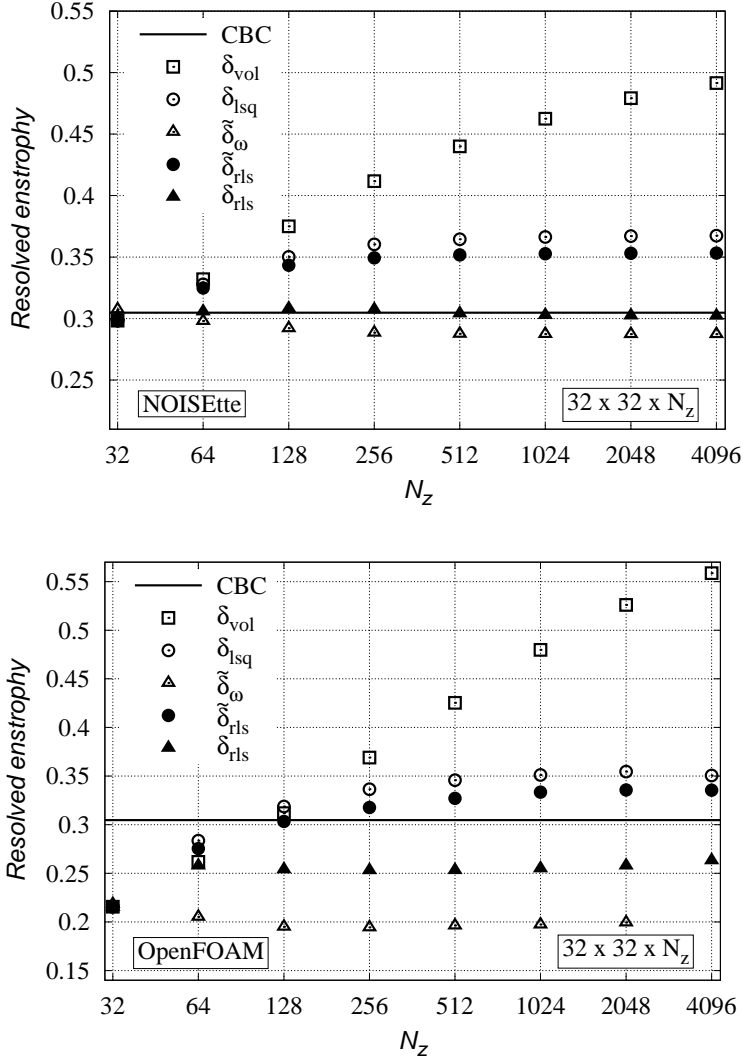


FIG. 10: Same as Figure 8 (bottom). In this case, results were obtained with two different codes: the in-house NOISEtte code (top) and OpenFOAM (bottom). Moreover, in addition to δ_{vol} and δ_{rls} (also shown in Figure 8), results include definitions of δ that depend on the flow topology: δ_{lsq} , $\tilde{\delta}_{\omega}$, and the newly proposed definition, $\tilde{\delta}_{rls}$.

The analysis is further extended in Figures 9 and 10 by considering length scales that depend on the local flow topology; namely, δ_{lsq} , $\tilde{\delta}_{\omega}$ and the newly proposed $\tilde{\delta}_{rls}$ and δ_{rls} . We selected $\tilde{\delta}_{\omega}$ because it was originally introduced as an improvement over the definition by Chauvet *et al.*³³ given in Eq.(10). On the other hand, the definition proposed by Shure *et al.*³⁶, δ_{SLA} , given in Eq. (12), has not been considered in this analysis, as it is a modified version of $\tilde{\delta}_{\omega}$ specifically tailored to trigger the Kelvin-Helmholtz instability in the early stages of shear

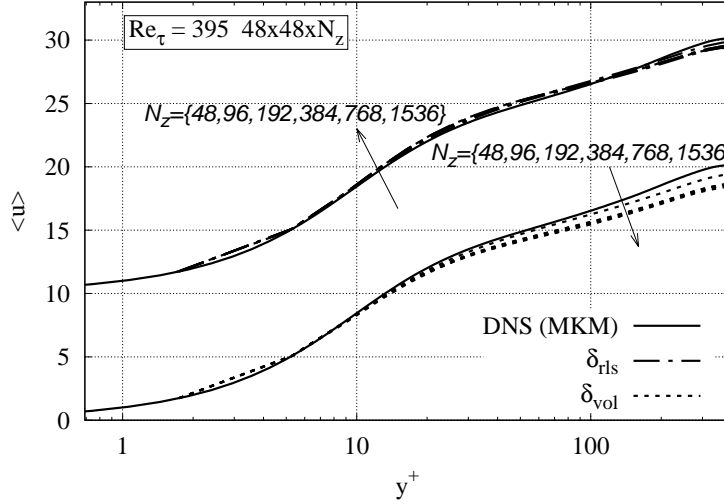


FIG. 11: Mean velocity, $\langle u \rangle$, for a turbulent channel flow at $Re_\tau = 395$ obtained for a set of anisotropic meshes $48 \times 48 \times N_z$ with $N_z = \{48, 96, 192, 384, 768, 1536\}$. Solid lines corresponds to the DNS results by Moser *et al.*⁵³. LES results obtained using the novel definition, δ_{rls} , are compared against those using δ_{vol} , with both employing the S3QR model²⁰. For clarity, the former results are shifted up.

layers. Apart from this, notice that, although the (face) evaluation of δ_{rls} does not depend on the local flow topology, its practical effect of the SGS models does depend. Therefore, it is also considered in this analysis. Moreover, for comparison, δ_{vol} is also included, as it represents the standard length scale used in the community. Again, it is remarkable the performance of δ_{rls} on highly anisotropic grids, showing even more robust results than the best flow-dependent definitions such as $\tilde{\delta}_\omega$. This is specially clear in the enstrophy analysis displayed in Figure 10. Apart from this, we can also observe that $\tilde{\delta}_{rls}$ has a very similar behavior as δ_{lsq} , constituting an excellent alternative to δ_{rls} if the SGS model is implemented following the standard approach. Finally, we can conclude that the newly proposed approach δ_{rls} displayed the best results among all the existing length scale definitions. This is even more remarkable when considering the simplicity of this new approach compared with the complexity of other alternatives such as $\tilde{\delta}_\omega$ and δ_{SLA} .

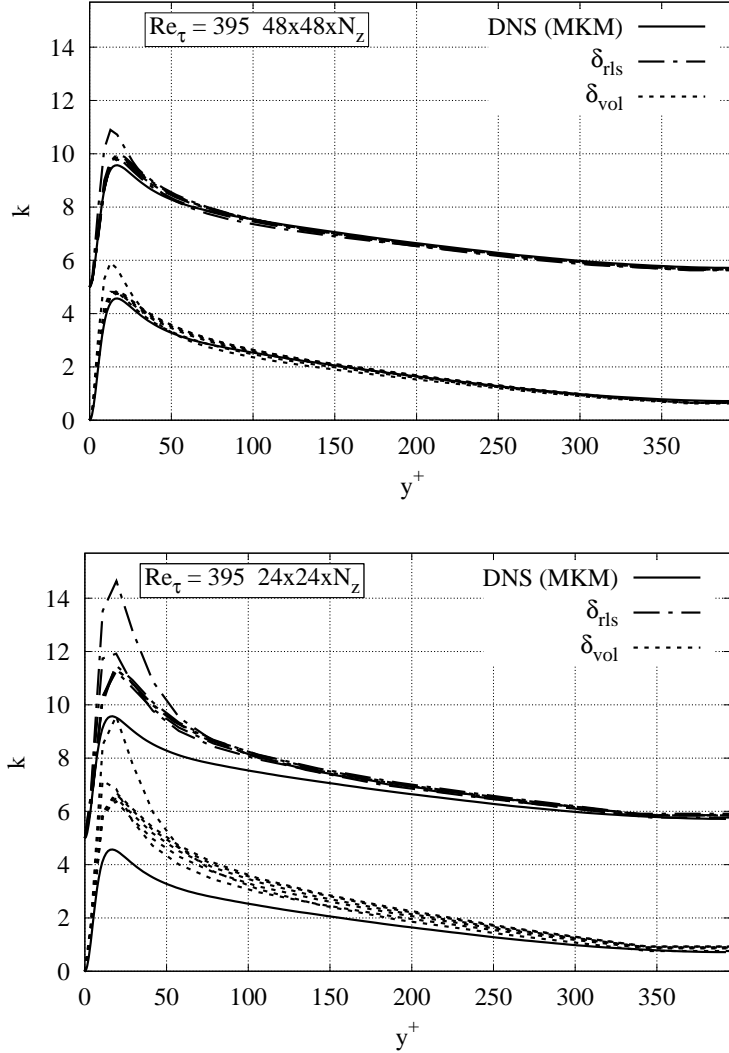


FIG. 12: Same as in Figure 11 but for the turbulent kinetic energy, k . In this case, two sets of anisotropic meshes have been analyzed. Top: $48 \times 48 \times N_z$ with $N_z = \{48, 96, 192, 384, 768, 1536\}$. Bottom: $24 \times 24 \times N_z$ with $N_z = \{24, 48, 96, 192, 384, 768\}$.

D. Turbulent channel flow

Finally, to assess the performance of the new definition δ_{rls} in the presence of walls, we consider a turbulent channel flow at $Re_\tau = 395$. For clarity, this test compares only δ_{rls} , which has demonstrated superior results over other alternatives including $\tilde{\delta}_{\text{rls}}$, against the standard length scale δ_{vol} . The simulations are performed using a code based on a symmetry-preserving finite-volume discretization⁵⁴ of the incompressible NS equations. The

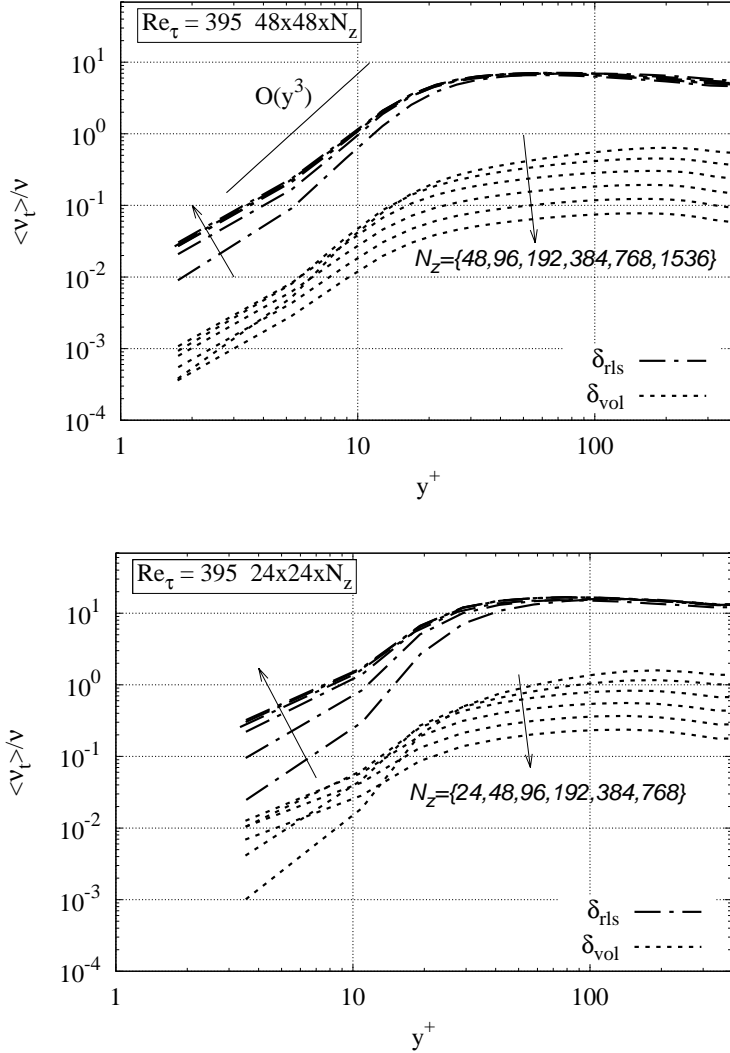


FIG. 13: Same as in Figure 12 but for the ratio between the average turbulent viscosity, $\langle \nu_t \rangle$, and the molecular viscosity, ν .

Smagorinsky model is not suitable for this case due to its inability to correctly capture the near-wall scaling of the turbulent viscosity⁵⁵, *i.e.*, $\nu_t \propto y^3$. Therefore, it has been replaced by the S3QR model, proposed in a previous work²⁰. Namely,

$$\nu_t^{S3QR} = (C_{s3qr}\delta)^2 Q_{GG^T}^{-1} R_{GG^T}^{5/6}, \quad (38)$$

where $C_{s3qr} = 0.762$, Q_{GG^T} and R_{GG^T} are the second and third invariants of the symmetric second-order tensor GG^T .

Figure 11 shows the average velocity profiles obtained for a set of (artificially) refined meshes in the span-wise direction, with resolutions of $48 \times 48 \times N_z$ and $N_z =$

{48, 96, 192, 384, 768, 1536}. Refinement is applied in the span-wise direction because the results are expected to be less sensitive to resolution in this direction compared to the stream-wise and wall-normal directions. LES results are compared with the DNS data by Moser *et al.*⁵³, and the channel dimensions are set to match those of the DNS, *i.e.*, $2\pi \times 2 \times \pi$. The grid is uniform in both the stream-wise and span-wise directions, while the wall-normal grid points are distributed using a hyperbolic sine function given by

$$y_j = \sinh(\gamma j / N_y) / \sinh(\gamma / 2) \quad j = 0, 1, \dots, N_y / 2. \quad (39)$$

Here, N_y is the number of grid points in the wall-normal direction, and the stretching parameter γ is set to 7. The grid points in the upper half of the channel are then obtained by symmetry. With this distribution and $N_y = 48$, the first off-wall grid point is located at $y^+ \approx 1.75$, *i.e.*, within the viscous sublayer ($y^+ < 5$). The corresponding resolutions are $\Delta x^+ \approx 51.7$ and $\Delta z^+ \approx 25.9$ (for $N_z = 48$). Therefore, the mesh is highly anisotropic near the wall, with, for instance, $\Delta x^+ / \Delta y^+ \approx 14.8$ in the first off-wall control volume.

As already observed in the homogeneous isotropic turbulence test-case, the results in Figure 11 confirm that the new definition of δ_{rls} exhibits significantly greater robustness to mesh anisotropy. Notably, the mean velocity profile remains virtually unchanged across all mesh refinements when using the proposed length scale, whereas substantial variations are observed with the standard definition δ_{vol} . A similar trend is observed in Figure 12 for the resolved turbulent kinetic energy, k , particularly in the bulk region, where the results obtained with δ_{rls} show minimal dependence on the value of N_z . This figure also includes results for a grid twice coarser on each spatial direction, *i.e.*, $24 \times 24 \times N_z$, with $N_z = \{24, 48, 96, 192, 384, 768\}$, shown at the bottom of the Figure 12. Although the resolution is insufficient for accurate prediction, the robustness of the new length scale under such coarse conditions is particularly remarkable.

Finally, Figure 13 presents the ratio between the time-averaged turbulent viscosity, $\langle \nu_t \rangle$, and the molecular viscosity, ν . These results provide valuable insight into the behavior of both length scale definitions. Specifically, δ_{rls} consistently yields similar values of $\langle \nu_t \rangle$ regardless of the resolution in the span-wise direction, while δ_{vol} clearly tends to switch off the SGS model as N_z increases. This contrasting behavior is especially evident in the bulk region of the channel. On the other hand, in the near-wall region, the ν_t tends to vanish towards the wall following the correct cubic behavior, *i.e.*, $\nu_t \propto y^3$ (see Figure 13,

top). Notice that the number of grid points in the wall-normal direction is insufficient to properly capture this behavior for the coarsest mesh (see Figure 13, bottom). In this region, noticeable differences persist for both δ_{rls} and δ_{vol} as the mesh is refined in the span-wise direction. At first sight, δ_{vol} tends to predict lower values of $\langle \nu_t \rangle$ with increasing N_z , while δ_{rls} shows the opposite trend. Nevertheless, the values of $\langle \nu_t \rangle$ predicted by δ_{rls} converge rapidly and monotonically with grid refinement.

In summary, the turbulent channel flow test confirms the robustness of the proposed length scale, δ_{rls} , in wall-bounded configurations with strong mesh anisotropy. The results show that δ_{rls} provides consistent predictions for mean velocity, turbulent kinetic energy, and turbulent viscosity across a wide range of span-wise resolutions. In contrast, the standard definition δ_{vol} exhibits significant sensitivity to mesh refinement, particularly in the bulk region where it tends to prematurely deactivate the SGS model. These findings further support the suitability of δ_{rls} as a simple and reliable subgrid characteristic length for LES simulations, including near-wall regions.

V. CONCLUDING REMARKS

This work proposes a novel definition of the subgrid characteristic length, δ , aimed at addressing the following research question: *can we establish a simple, robust, and easily implementable definition of δ for any type of grid that minimizes the impact of mesh anisotropies on the performance of SGS models for LES?* The motivation stems from the widespread use of the Deardorff definition (see Eq. 4), *i.e.*, the cube root of the cell volume, even though it is known to perform poorly on highly anisotropic grids.

In this context, we argue that the proposed *rational length scale*, δ_{rls} , defined in Eq. (30), is an excellent alternative. It naturally emerges from the entanglement between numerical discretization and LES filtering. Furthermore, its favorable mathematical properties and simplicity indicate that it is a robust and reliable choice, effectively reducing the impact of mesh anisotropies on simulation accuracy. Specifically, it is locally defined, frame-invariant, and well-bounded (see properties **P1** and **P2** in Section IV A), well-conditioned, and has a very low computational cost (property **P6**). Additionally, it is suitable for unstructured meshes (property **P4**) and is computed directly at cell faces (property **P5**). This latter

feature is a distinctive characteristic that sets δ_{rls} apart from other length scale definitions (see Table II). Therefore, it requires a couple of very simple modifications respect to the standard implementation of an eddy-viscosity model (see Figure 3c). Note that although δ_{rls} has been derived within the framework of a second-order FVM, a similar derivation could be applied to other existing spatial discretization approaches. Therefore, the proposed method is not restricted to FVM.

Additionally, the alternative dissipation-equivalent definition, $\tilde{\delta}_{\text{rls}}$, given in Eq. (34), has also been proposed. Like other existing definitions, $\tilde{\delta}_{\text{rls}}$ is evaluated at the cell centers. Furthermore, this length scale depends on the local flow topology characterized by the gradient of the resolved velocity, $\mathbf{G} \equiv \nabla \mathbf{u}$ (property **P3**). Regarding this, analytical studies of simple flow configurations indicate the suitability of the proposed definitions.

Numerical results have demonstrated the effectiveness of the proposed subgrid characteristic length scales through simulations of decaying isotropic turbulence using two different codes. Comparisons with Deardorff’s classical definition, δ_{vol} , confirm that both new approaches, $\tilde{\delta}_{\text{rls}}$ and δ_{rls} , are significantly more robust to mesh anisotropies. While both perform well, δ_{rls} consistently exhibits greater robustness in highly anisotropic configurations. This improved behavior has also been confirmed in a turbulent channel flow at $Re_\tau = 395$, further supporting its applicability in practical LES settings. Given its favorable mathematical properties, ease of implementation, and minimal computational overhead, we conclude that δ_{rls} is a reliable and broadly applicable choice for SGS modeling in complex geometries, including those involving highly skewed or unstructured meshes.

Finally, it is worth mentioning that the selection of the appropriate turbulent length scale is of crucial importance for hybrid RANS-LES approaches, particularly in the context of DES. As demonstrated in our previous research⁴³, a SGS model that provides very good GAM properties was unable to guarantee a proper solution in the regions of resolved turbulence on anisotropic meshes. This is of particular significance for aeroacoustics⁴⁴, where deficiencies in the simulation of resolved turbulence dynamics can have a substantial impact. The *rational length scale* thus emerges as a promising candidate for use in DES simulations as well.

ACKNOWLEDGEMENTS

F.X.T. and J.R. are supported by SIMEX project (PID2022-142174OB-I00) of the *Ministerio de Ciencia e Innovación* MCIN/AEI/ 10.13039/501100011033 and the European Union Next GenerationEU. Calculations were carried out on the MareNostrum 5-GPP supercomputer at BSC. We thankfully acknowledge these institutions.

REFERENCES

- ¹D. K. Lilly. The representation of small scale turbulence in numerical simulation experiments. In H. H. Goldstine, editor, *IBM Scientific Computing Symposium on Environmental Sciences*, pages 195–210, Yorktown Heights, NY:IBM, 1967.
- ²J. Smagorinsky. General Circulation Experiments with the Primitive Equations. *Monthly Weather Review*, 91:99–164, 1963.
- ³P. Moin and J. Kim. Numerical investigations of turbulent channel flow. *Journal of Fluid Mechanics*, 118:341–377, 1982.
- ⁴U. Piomelli, J. Ferziger, P. Moin, and J. Kim. New approximate boundary conditions for large eddy simulations of wall-bounded flows. *Physics of Fluids A*, 1:1061–1068, 1989.
- ⁵M. Germano, U. Piomelli, P. Moin, and W. H. Cabot. A dynamic subgrid-scale eddy viscosity model. *Physics of Fluids*, 3:1760–1765, July 1991.
- ⁶D. K. Lilly. A proposed modification of the Germano subgrid-scale closure method. *Physics of Fluids A*, 4:633–635, 1992.
- ⁷S. Ghosal, T. S. Lund, P. Moin, and K. Akselvoll. A dynamic localization model for large-eddy simulation of turbulent flows. *Journal of Fluid Mechanics*, 286:229–255, 1995.
- ⁸C. Meneveau, T. S. Lund, and W. H. Cabot. A Lagrangian dynamic subgrid-scale model of turbulence. *Journal of Fluid Mechanics*, 319:353–385, 1996.
- ⁹N. Park, S. Lee, J. Lee, and H. Choi. A dynamic subgrid-scale eddy viscosity model with a global model coefficient. *Physics of Fluids*, 18(12):125109, 2006.
- ¹⁰M. Germano. Turbulence: the filtering approach. *Journal of Fluid Mechanics*, 238:325–336, 1992.
- ¹¹D. You and P. Moin. A dynamic global-coefficient subgrid-scale eddy-viscosity model for large-eddy simulation in complex geometries. *Physics of Fluids*, 19(6):065110, 2007.

- ¹²A. E. Tejada-Martínez and K. E. Jansen. A dynamic Smagorinsky model with dynamic determination of the filter width ratio. *Physics of Fluids*, 16(7):2514–2528, 2004.
- ¹³A. E. Tejada-Martínez and K. E. Jansen. A parameter-free dynamic subgrid-scale model for large-eddy simulation. *Computer Methods in Applied Mechanics and Engineering*, 195:2919–2938, 2006.
- ¹⁴F. Nicoud and F. Ducros. Subgrid-scale stress modelling based on the square of the velocity gradient tensor. *Flow, Turbulence and Combustion*, 62(3):183–200, 1999.
- ¹⁵A. W. Vreman. An eddy-viscosity subgrid-scale model for turbulent shear flow: Algebraic theory and applications. *Physics of Fluids*, 16(10):3670–3681, 2004.
- ¹⁶F. Nicoud, H. B. Toda, O. Cabrit, S. Bose, and J. Lee. Using singular values to build a subgrid-scale model for large eddy simulations. *Physics of Fluids*, 23(8):085106, 2011.
- ¹⁷R. Verstappen. When does eddy viscosity damp subfilter scales sufficiently? *Journal of Scientific Computing*, 49(1):94–110, 2011.
- ¹⁸W. Rozema, H. J. Bae, P. Moin, and R. Verstappen. Minimum-dissipation models for large-eddy simulation. *Physics of Fluids*, 27:085107, 2015.
- ¹⁹S. Ryu and G. Iaccarino. A subgrid-scale eddy-viscosity model based on the volumetric strain-stretching. *Physics of Fluids*, 26(6):065107, 2014.
- ²⁰F. X. Trias, D. Folch, A. Gorobets, and A. Oliva. Building proper invariants for eddy-viscosity subgrid-scale models. *Physics of Fluids*, 27(6):065103, 2015.
- ²¹M. H. Silvis, R. A. Remmerswaal, and R. Verstappen. Physical consistency of subgrid-scale models for large-eddy simulation of incompressible turbulent flows. *Physics of Fluids*, 29(1):015105, 2017.
- ²²J. Hasslberger, M. Reissmann, R. D. Sandberg, and M. Klein. Exploiting semantic back-propagation to impose near-wall scaling constraints in machine-learned symbolic subgrid-scale closures. *Physics of Fluids*, 37(3), 2025.
- ²³J. W. Deardorff. Numerical study of three-dimensional turbulent channel flow at large Reynolds numbers. *Journal of Fluid Mechanics*, 41:453–480, 1970.
- ²⁴U. Schumann. Subgrid scale model for finite difference simulations of turbulent flows in plane channels and annuli. *Journal of Computational Physics*, 18:376–404, 1975.
- ²⁵D. K. Lilly. The length scale for sub-grid-scale parametrization with anisotropic resolution. *Center for Turbulence Research, Annual Research Briefs*, 1998.

- ²⁶A. Scotti, C. Meneveau, and D. K. Lilly. Generalized Smagorinsky model for anisotropic grids. *Physics of Fluids A*, 5(9):2306–2308, 1993.
- ²⁷A. Scotti, C. Meneveau, and M. Fatica. Dynamics Smagorinsky model on anisotropic grids. *Physics of Fluids*, 9(6):1856–1858, 1997.
- ²⁸C. E. Colosqui and A. A. Oberai. Generalized Smagorinsky model in physical space. *Computers & Fluids*, 37:207–217, 2008.
- ²⁹A. Prakash, K. Jansen, and J. Evans. Invariant data-driven subgrid stress modeling on anisotropic grids for large eddy simulation. *Computer Methods in Applied Mechanics and Engineering*, 422:116807, 2024.
- ³⁰N. Chang, Z. Yuan, Y. Wang, and J. Wang. The effect of filter anisotropy on the large eddy simulation of turbulence. *Physics of Fluids*, 35(3), 2023.
- ³¹J. Schumann, S. Toosi, and J. Larsson. Assessment of grid anisotropy effects on large-eddy-simulation models with different length scales. *AIAA Journal*, 58(10):4522 – 4533, 2020.
- ³²P. R. Spalart, W. H. Jou, M. Strelets, and S. R. Allmaras. Comments on the feasibility of LES for wings, and on a hybrid RANS/LES approach. In *C. Liu & Z. Liu (eds.) Advances in DES/LES*. Greyden Press, Columbus, OH, 1997.
- ³³N. Chauvet, S. Deck, and L. Jacquin. Zonal detached eddy simulation of a controlled propulsive jet. *AIAA Journal*, 45(10):2458–2473, 2007.
- ³⁴S. Deck. Recent improvements in the Zonal Detached Eddy Simulation (ZDES) formulation. *Theoretical and Computational Fluid Dynamics*, 26(6):523–550, 2012.
- ³⁵C. Mockett, M. Fuchs, A. Garbaruk, M. Shur, P. Spalart, M. Strelets, F. Thiele, and A. Travin. Two Non-zonal Approaches to Accelerate RANS to LES Transition of Free Shear Layers in DES. In Sharath Girimaji, Werner Haase, Shia-Hui Peng, and Dieter Schwamborn, editors, *Progress in Hybrid RANS-LES Modelling*, volume 130 of *Notes on Numerical Fluid Mechanics and Multidisciplinary Design*, pages 187–201. Springer International Publishing, 2015.
- ³⁶M. L. Shur, P. R. Spalart, M. K. Strelets, and A. K. Travin. An Enhanced Version of DES with Rapid Transition from RANS to LES in Separated Flows. *Flow, Turbulence and Combustion*, 95:709–737, 2015.
- ³⁷E. Guseva, A. Garbaruk, and M. Strelets. Assessment of Delayed DES and Improved Delayed DES Combined with a Shear-Layer-Adapted Subgrid Length-Scale in Separated

- Flows. *Flow, Turbulence and Combustion*, 98(2):481 – 502, 2017.
- ³⁸M. Xiao and Y. Zhang. Assessment of the SST-IDDES with a shear-layer-adapted subgrid length scale for attached and separated flows. *International Journal of Heat and Fluid Flow*, 85, 2020.
- ³⁹Z. Zhou, M. Xiao, D. Li, and Y. Zhang. Enhanced delayed detached-eddy simulation with anisotropic minimum dissipation subgrid length scale. *Physics of Fluids*, 37(2), 2025.
- ⁴⁰X. Zhang, M. Savoie, M. Quinn, B. Parslew, and A. Revell. Simulation of flow around a finite rectangular prism: influence of mesh, model, and subgrid length scale. *Entropy*, 27(1), 2025.
- ⁴¹F. X. Trias, A. Gorobets, M. H. Silvis, R. W. C. P. Verstappen, and A. Oliva. A new subgrid characteristic length for turbulence simulations on anisotropic grids. *Physics of Fluids*, 26:115109, 2017.
- ⁴²R. A. Clark, J. H. Ferziger, and W. C. Reynolds. Evaluation of subgrid-scale models using an accurately simulated turbulent flow. *Journal Fluid Mechanics*, 91:1–16, 1979.
- ⁴³A. Pont-Vílchez, A. Duben, A. Gorobets, A. Revell, A. Oliva, and F. X. Trias. New strategies for mitigating the Grey Area in DDES models. *AIAA Journal*, 59(9):3331–3345, 2021.
- ⁴⁴A. Duben, J. Ruano, A. Gorobets, J. Rigola, and F. X. Trias. Evaluation of enhanced gray area mitigation approaches based on jet aeroacoustics. *AIAA Journal*, 61(2), 2023.
- ⁴⁵F. X. Trias, O. Lehmkuhl, A. Oliva, C.D. Pérez-Segarra, and R.W.C.P. Verstappen. Symmetry-preserving discretization of Navier-Stokes equations on collocated unstructured meshes. *Journal of Computational Physics*, 258:246–267, 2014.
- ⁴⁶F. X. Trias, X. Álvarez-Farré, À. Alsalti-Baldellou, A. Gorobets, and A. Oliva. An efficient eigenvalue bounding method: CFL condition revisited. *Computer Physics Communications*, 305:109351, 2024.
- ⁴⁷P. Sagaut. *Large Eddy Simulation for Incompressible Flows: An Introduction*. Springer, 3rd edition, 2005.
- ⁴⁸G. Comte-Bellot and S. Corrsin. Simple Eulerian time correlation of full- and narrow-band velocity signals in grid-generated, isotropic turbulence. *Journal of Fluid Mechanics*, 48:273–337, 1971.
- ⁴⁹A. Gorobets and P. Bakhvalov. Heterogeneous CPU+GPU parallelization for high-accuracy scale-resolving simulations of compressible turbulent flows on hybrid supercom-

- puters. *Computer Physics Communications*, 271:108231, 2022.
- ⁵⁰I. Abalakin, P. Bakhvalov, V. Bobkov, A. Duben, A. Gorobets, T. Kozubskaya, P. Rodionov, and N. Zhdanova. NOISEtte CFD&CAA Supercomputer Code for Research and Applications. *Supercomputing Frontiers and Innovations*, 11(2):78 – 101, 2024.
- ⁵¹I. Abalakin, P. Bakhvalov, and T. Kozubskaya. Edge-based reconstruction schemes for unstructured tetrahedral meshes. *International Journal for Numerical Methods in Fluids*, 81(6):331–356, 2016.
- ⁵²J. Ruano. DHIT GitHub Page: <https://github.com/jruanoperez/DHIT>, 2025.
- ⁵³R. D. Moser, J. Kim, and N. N. Mansour. Direct numerical simulation of turbulent channel flow up to $Re_\tau = 590$. *Physics of Fluids*, 11:943–945, 1999.
- ⁵⁴R. W. C. P. Verstappen and A. E. P. Veldman. Symmetry-Preserving Discretization of Turbulent Flow. *Journal of Computational Physics*, 187:343–368, 2003.
- ⁵⁵D. R. Chapman and G. D. Kuhn. The limiting behaviour of turbulence near a wall. *Journal of Fluid Mechanics*, 170:265–292, 1986.